# On the Phase Reduction and Response Dynamics of Neural Oscillator Populations

**Eric Brown**
*ebrown@math.princeton.edu*
**Jeff Moehlis**\*
*jmoehlis@math.princeton.edu*
*Program in Applied and Computational Mathematics, Princeton University,*
*Princeton, NJ 08544, U.S.A.*

**Philip Holmes**
*pholmes@math.princeton.edu*
*Program in Applied and Computational Mathematics and Department of Mechanical*
*and Aerospace Engineering, Princeton University, Princeton, NJ 08544, U.S.A.*

**We undertake a probabilistic analysis of the response of repetitively firing neural populations to simple pulselike stimuli. Recalling and extending results from the literature, we compute phase response curves (PRCs) valid near bifurcations to periodic firing for Hindmarsh-Rose, Hodgkin-Huxley, FitzHugh-Nagumo, and Morris-Lecar models, encompassing the four generic (codimension one) bifurcations. Phase density equations are then used to analyze the role of the bifurcation, and the resulting PRC, in responses to stimuli. In particular, we explore the interplay among stimulus duration, baseline firing frequency, and population-level response patterns. We interpret the results in terms of the signal processing measure of gain and discuss further applications and experimentally testable predictions.**

## 1 Introduction

This letter seeks to add to our understanding of how the firing rates of populations of neural oscillators respond to pulselike stimuli representing sensory inputs and to connect this to mechanisms of neural computation and modulation. In particular, we study how responses depend on oscillator type (classified by its bifurcation to periodic firing), baseline firing rate of the population, and duration of the input. As in, e.g., Fetz and Gustaffson (1983) and Herrmann and Gerstner (2001), our results also apply to the interpretation of peri-stimulus time histograms (PSTHs), which represent averages over ensembles of independent neuronal recordings.

---

   \* Current address: Department of Mechanical and Environmental Engineering, University of California, Santa Barbara, CA 93106 U.S.A.

We are motivated by attempts to understand different responses, in the form of PSTHs of spike rates in the brainstem organ locus coeruleus, of monkeys performing target identification and other tasks (Usher, Cohen, Servan-Schreiber, Rajkowsky, & Aston-Jones, 1999; Brown, Mohelis, Holmes, Clayton, Rajkowski, & Aston-Jones, 2003b), but there are many other situations in which populations of spiking neurons are reset by stimuli. For example, the multiple oscillator and beat frequency models of interval timing of Meck et al. (Matell & Meck, 2000) involve cortical oscillators of differing frequencies, and the 40 Hz synchrony reported by Gray and Singer and Eckhorn et al. (see Gray, 2000, and Eckhorn, 1999, for reviews) also suggest the onset of coherent oscillations in visual cortex.

For most neuron models, we find that the response of populations to a fixed stimulus current scales inversely with the prestimulus baseline firing rate of the population. While the firing rates of individual neurons also display this inverse relationship (encoded in their $f - I$ curves; Rinzel & Ermentrout, 1998), the scaling of the population response differs from that of individual neurons. This effect suggests a possible role of baseline firing rate in cognitive processing by neural populations: decreasing baseline firing rates (via reduced inputs from other brain areas or via neuromodulators; e.g. Usher et al., 1999; Aston-Jones, Rajkowski, & Cohen, 2000; Aston-Jones, Chen, Zhu, & Oshinsky, 2001) can adjust the 'fraction' of an incoming stimulus that is passed on to the next processing module. Recent data from the brainstem nucleus locus coeruleus (LC), for example, reflect this pattern: greater responsivity and better cognitive performance are both correlated with slower baseline firing rates (Aston-Jones, Rajkowski, Kubiak, & Alexinsky, 1994; Usher et al., 1999; Brown et al., 2003b).

We also find that for certain common neuron models, the maximum population response to a step stimulus of fixed strength can occur only (if it occurs at all) *after* stimulus removal. Moreover, in all cases, there are resonant stimulus durations for which there is no poststimulus response. Thus, the magnitude and timing of maximal population response depends strongly on both neuron type and stimulus duration relative to the baseline period.

This letter is organized as follows. Section 2 discusses phase reduction techniques for ordinary differential equations with attracting limit cycles. In the following section, we recall and compute phase response curves for familiar neuron models near the four codimension one bifurcations to periodic firing, using normal forms and numerical calculations (Ermentrout, 2002). These two sections review part of the broad literature on the topic and provide new results: PRCs valid near degenerate Hopf and homoclinic bifurcations and the scaling of PRCs with the frequency of the neurons from which they are derived. Section 4 then analyzes firing probabilities in response to simple stimuli, enabling us to predict spike histograms, describe their dependence on parameters characterizing the stimuli and neuron type, and emphasize similarities and differences among the responses of different models. These results are summarized in six roman-numbered boldface

statements. Section 5 interprets these results in terms of the gain, or signal amplification, of neural populations. Section 6 closes the letter with comments on further applications and possible experimental tests.

Both phase reduction methods and population modeling have a rich history, including numerous applications in neuroscience. The classical phase coordinate transformation used in this article originated at least by 1949 (Malkin, 1949), with the complementary asymptotic phase ideas expanded in, among others, Coddington and Levinson (1955), Winfree (1974, 2001), and Guckenheimer (1975) and applied in Ermentrout and Kopell (1984, 1990, 1991), Hansel, Mato, and Meunier (1993, 1995), van Vreeswijk, Abbott, and Ermentrout (1994), Ermentrout (1996), Hoppensteadt and Izhikevich (1997), Kuramoto (1997), Kim and Lee (2000), Bressloff and Coombes (2000), Izhikevich (2000b), Brown, Holmes, and Moehlis (2003a), and Lewis and Rinzel (2003); see also the related "spike response method" in Gerstner, van Hemmen, & Cowan, 1996, and Gerstner & Kistler, 2002 and references therein.

Voltage density approaches, primarily undertaken in an integrate-and-fire framework involving reinjection boundary conditions and in some cases involving distributed conductances, are developed and applied in, among others, Stein (1965), Wilson and Cowan (1972), Fetz and Gustaffson (1983), Gerstner (2000), Nykamp and Tranchina (2000), Omurtag, Knight, and Sirovich (2000), Herrmann and Gerstner (2001), Casti et al. (2001), Brunel, Chance, Fourcaud, and Abbott (2001), Fourcaud and Brunel (2002), and Gerstner and Kistler (2002). In particular, density formulations derived from integrate-and-fire models (Fetz & Gustaffson, 1983; Herrmann & Gerstner, 2001) demonstrate the inverse relationship between peak firing rates and baseline frequency (for populations receiving pulsed stimuli) that we extend to other neuron models in this article. The work of Brunel et al. (2001) and Fourcaud and Brunel (2002) focusses on the transmission of stimuli by noisy integrate-and-fire populations. It explains how components of incoming signals are shifted and attenuated (or amplified) when output as firing rates of the population, depending on the frequency of the signal component and the characteristics of noise in the population. Some of the conclusions of our article (for integrate-and-fire neurons only) could presumably be reconstructed from the Brunel et al. results by decomposing our stepped stimuli into Fourier components; however, simpler methods applicable to our noise-free case allow our different analytical insights into response properties. Experiments on population responses to applied stepped and fluctuating currents have also been performed, for example, by Mainen and Sejnowski (1995) in cortical neurons. Due to noise inherent in their biological preparations, responses to stepped, but not fluctuating, stimuli are gradually damped (cf. also Gerstner, 2000; Gerstner & Kistler, 2002); these effects are studied using a phase density approach by Ritt (2003).

The phase density formulation is also used in Kuramoto (1984) and Strogatz (2000), where the emphasis is on coupling effects in populations with distributed frequencies, generally without external stimuli. The approach

closest to ours is that of Tass (1999), who focuses on how pulsed input signals can desynchronize populations of noisy, coupled phase oscillators that have clustered equilibrium states; of particular interest is the critical stimulus duration $T_{crit}$ for which the maximum desynchronizing effect is achieved. By contrast, this letter focuses on synchronizing responses of independent noiseless oscillators (with uniform stationary distributions) and, using analytical solutions to this simpler problem, stresses the influence of individual neuron properties. Specifically, we contribute a family of simple expressions for time-dependent firing rates in response to pulsed stimuli, derived from different nonlinear oscillator models via phase reductions and the method of characteristics. Our expressions allow us to identify a series of novel relationships between population dynamics during and after stepped stimuli and the frequencies and bifurcation types of the individual neurons making up the population. As already mentioned, we consider only uncoupled (and noiseless) neurons, but we note that our results remain generally valid for weakly coupled systems. In particular, in Brown et al. (2003b), we show that for a noisy neural population with synaptic and electrotonic couplings sufficient to reproduce observed variations in experimental cross-correlograms, the uncoupled limit is adequate for understanding key first-order modulatory effects.

## 2 Phase Equations for Nonlinear Oscillators with Attracting Limit Cycles

**2.1 Phase Reductions.** Following, e.g., Ermentrout (1996, 2002), Hoppensteadt and Izhikevich (1997), Guckenheimer (1975), and Winfree (1974, 2001), we first describe a coordinate change to phase variables that will simplify the analysis to come. Our starting point is a general, conductance-based model of a single neuron:

$$C\dot{V} = [I^g(V, \mathbf{n}) + I^b + I(V, t)], \tag{2.1}$$

$$\dot{\mathbf{n}} = \mathbf{N}(V, \mathbf{n}); (V, \mathbf{n})^T \in \mathbb{R}^N. \tag{2.2}$$

Here, $V$ is the voltage difference across the membrane, the $(N-1)$-dimensional vector $\mathbf{n}$ comprises gating variables and $I^g(V, \mathbf{n})$ the associated membrane currents, and $C$ is the cell membrane capacitance. The baseline inward current $I^b$ effectively sets oscillator frequency and will correspond below to a bifurcation parameter. $I(V, t)$ represents synaptic currents from other brain areas due to stimulus presentation; below, we neglect reversal potentials so that $I(V, t) = I(t)$. We write this equation in the general form

$$\dot{\mathbf{x}} = F(\mathbf{x}) + G(\mathbf{x}, t); \qquad \mathbf{x} = (V, \mathbf{n})^T \in \mathbb{R}^N, \tag{2.3}$$

where $F(\mathbf{x})$ is the baseline vector field, $G(\mathbf{x}, t)$ is the stimulus effect, and $^T$ denotes transpose. In our simplification, $G(\mathbf{x}, t) = (I(t), \mathbf{0})^T$; in a more general setting, perturbations in the gating equations 2.2, could also be included.

We assume that the baseline ($G \equiv 0$) neural oscillator has a normally hyperbolic (Guckenheimer & Holmes, 1983), attracting limit cycle $\gamma$. This persists under small perturbations (Fenichel, 1971), and hereafter we assume that such a limit cycle always exists for each neuron.

The objective is to simplify equation 2.3 by defining a scalar phase variable $\theta(\mathbf{x}) \in [0, 2\pi)$ for all $\mathbf{x}$ in some neighborhood $U$ of $\gamma$ (within its domain of attraction), such that the phase evolution has the simple form $\frac{d\theta(\mathbf{x})}{dt} = \omega$ for all $\mathbf{x} \in U$ when $G \equiv 0$. Here, $\omega = 2\pi/T$, where $T$ is the period of equation 2.3 with $G \equiv 0$. From the chain rule, this requires

$$\frac{d\theta(\mathbf{x})}{dt} = \frac{\partial\theta}{\partial\mathbf{x}}(\mathbf{x}) \cdot F(\mathbf{x}) + \frac{\partial\theta}{\partial\mathbf{x}}(\mathbf{x}) \cdot G(\mathbf{x}, t) = \omega + \frac{\partial\theta}{\partial\mathbf{x}}(\mathbf{x}) \cdot G(\mathbf{x}, t) . \qquad (2.4)$$

Equation 2.4 defines a first-order partial differential equation (PDE) that the scalar field $\theta(\cdot)$ must satisfy. Using the classical techniques of isochrons (Winfree, 1974, 2001; Guckenheimer, 1975; Kuramoto, 1997; cf. Hirsch, Pugh, & Shub, 1977), the unique (up to a translational constant) solution $\theta(\cdot)$ to this PDE can be constructed indirectly.

Even after $\theta(\cdot)$ has been found (see the next subsection), equation 2.4 is not a phase-only (and hence self-contained) description of the oscillator dynamics. However, evaluating the vector field at $\mathbf{x}^\gamma(\theta)$, which we define as the intersection of $\gamma$ and the $\theta(\mathbf{x})$ level set (i.e., isochron), we have

$$\frac{d\theta(\mathbf{x})}{dt} = \omega + \frac{\partial\theta}{\partial\mathbf{x}}(\mathbf{x}^\gamma(\theta)) \cdot G(\mathbf{x}^\gamma(\theta, t)) + E , \qquad (2.5)$$

where $E$ is an error term of $\mathcal{O}(|G|^2)$, where the scalar $|G|$ bounds $G(\mathbf{x}, t)$ over all components as well as over $\mathbf{x}$ and $t$ (cf. Kuramoto, 1997).

Dropping this error term, we may rewrite equation 2.5 as the one-dimensional phase equation,

$$\frac{d\theta}{dt} = \omega + \frac{\partial\theta}{\partial\mathbf{x}}(\theta) \cdot G(\theta, t) , \qquad (2.6)$$

which is valid (up to the error term) in the whole neighborhood $U$ of $\gamma$.

## 2.2 Computing the Phase Response Curve.

In the case of equations 2.1 and 2.2, the only partial derivative we must compute to fully define equation 2.6 is with respect to voltage, and we define the *phase response curve* (PRC; Winfree, 2001) as $\frac{\partial\theta}{\partial V}(\theta) \equiv z(\theta)$. Then equation 2.6 becomes

$$\frac{d\theta}{dt} = \omega + z(\theta)I(t) \equiv v(\theta, t), \qquad (2.7)$$

the population dynamics of which is the subject of this letter. Note that
equation 2.7 neglects reversal potential effects for the various synapses that
contribute to the net $I(t)$: if these were included, $I(t)$ would be replaced by
$I(\theta, t)$. Furthermore, if $G$ had nonzero components in more than just the
voltage direction, we would need to compute a vector-valued PRC; each
component of this could be computed in a similar manner to that below.

*2.2.1 Direct Method.* We now describe a straightforward and classical
way to compute $z(\theta)$ that is useful in experimental, numerical, and analytical
studies (Winfree, 1974, 2001; Glass & Mackey, 1988; Kuramoto, 1997). By
definition,

$$z(\theta) = \lim_{\Delta V \to 0} \frac{\Delta\theta}{\Delta V}, \qquad (2.8)$$

where $\Delta\theta = \left[\theta(\mathbf{x}^\gamma + (\Delta V, \mathbf{0})^\mathbf{T}) - \theta(\mathbf{x}^\gamma)\right]$ is the change in $\theta(\mathbf{x})$ resulting from
a perturbation $V \to V + \Delta V$ from the base point $\mathbf{x}^\gamma$ on $\gamma$ (see Figure 1). Since
$\dot\theta = \omega$ everywhere in the neighborhood of $\gamma$, the difference $\Delta\theta$ is preserved
under the baseline ($G = 0$) phase flow; thus, it may be measured in the limit
as $t \to \infty$, when the perturbed trajectory has collapsed back to the limit
cycle $\gamma$. That is, $z(\theta)$ can be found by comparing the phases of solutions
in the infinite-time limit starting on and infinitesimally shifted from base
points on $\gamma$. This is the idea of asymptotic phase. This method will be used
in section 3 to compute PRCs for the normal forms commonly arising in
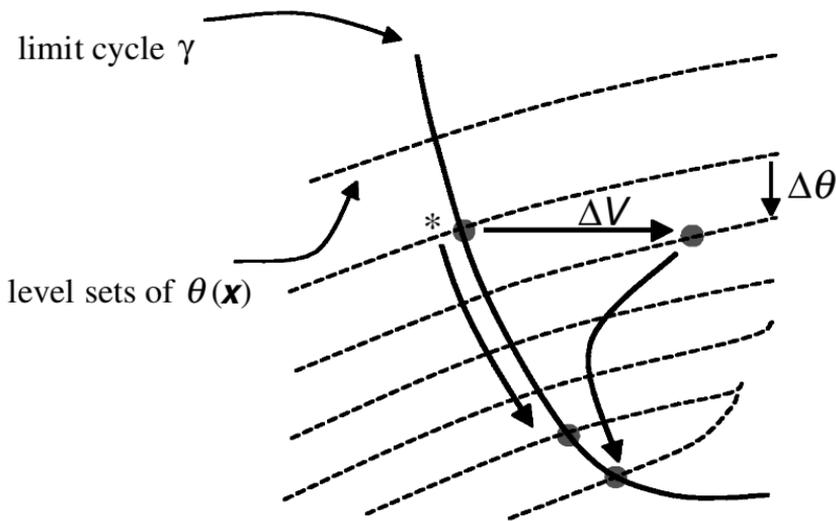neural models.



Figure 1: The direct method for computing $\frac{\partial\theta}{\partial V}$ at the point indicated by * is
to take the limit of $\Delta\theta/\Delta V$ for vanishingly small perturbations $\Delta V$. One can
calculate $\Delta\theta$ in the limit $t \to \infty$, as discussed in the text.

*2.2.2 Other Methods.* Another technique for finding $\frac{\partial\theta}{\partial V}(\theta)$ involves solving the adjoint problem associated with equations 2.1 and 2.2 (Hoppensteadt & Izhikevich, 1997; Ermentrout & Kopell, 1991); this procedure is automated in the program XPP (Ermentrout, 2002) and is equivalent to the direct method discussed above. This equivalence, described in appendix A, is implicit in the calculation of coupling functions presented in Hoppensteadt and Izhikevich (1997) and Ermentrout (2002). The implementation of the adjoint method on XPP is used to compute the PRCs for full neuron models that are compared with normal form predictions later in this article.

Since only partial derivatives $\frac{\partial\theta}{\partial\mathbf{x}}$ evaluated on $\gamma$ enter equation 2.7, and not the value of the phase function $\theta$ itself, it is tempting to compute these partial derivatives directly from equation 2.4. However, when viewed as an algebraic equation for the vector field $\frac{\partial\theta}{\partial\mathbf{x}}$, equation 2.4 yields infinitely many solutions, being only one equation for the $N$ unknown functions $\frac{\partial\theta}{\partial x_j}$, $j = 1, \ldots, N$. Some of these solutions are much easier to construct than the phase response curve computed via the direct or the adjoint method. However, for such a solution, which we write as $\frac{\partial\theta_2}{\partial\mathbf{x}}$ ($\neq \frac{\partial\theta}{\partial\mathbf{x}}$) to distinguish it from partial derivatives of the asymptotic phase $\theta$, there is not necessarily a corresponding phase variable $\theta_2$ such that $\frac{d\theta_2(\mathbf{x})}{dt} = \omega$, $\mathbf{x} \in \mathbf{U}$ (in the absence of stimulus): recall the uniqueness of the solution $\theta(\mathbf{x})$ to equation 2.4. (See appendix B for a specific coordinate change from the literature in this context.)

**2.3 Validity of the Phase Reduction.** We shall always assume that the phase flow $\dot{\theta}$ is nonnegative at the spike point $\theta_s \equiv 0$; otherwise equation 2.7 does not make sense as a neuron model (neurons cannot cross "backwards" through the spike and regain a state from which they can immediately fire again). For oscillators giving PRCs $z(\theta)$ with $z(\theta_s) \neq 0$, this assumption restricts admissible perturbing functions $I(t)$ (or, in the more general case of equation 2.6, $G(\mathbf{x}, t)$) to those satisfying

$$I(t)z(\theta_s) > -\omega. \tag{2.9}$$

Thus, for $z(\theta_s) > 0$, excitatory input ($I(t) > 0$) is always admissible, but there is a lower bound on the strength of inhibitory input for which phase reductions hold. In particular, if $I(t)$ contains a noise component, it must be bounded below; this requires trimming the white (diffusive) or Ornstein-Uhlenbeck noise processes commonly used to model variability in synaptic inputs. These problems do not arise for continuous PRCs having $z(\theta_s) = 0$.

We note that $z(\theta_s) = 0$ approximately holds for the Hodgkin-Huxley (HH) and Hindmarsh-Rose (HR) neurons to be considered below, and indeed holds for any neuron model with a fast vector field surrounding the spike tip $\mathbf{x_s}$ on the limit cycle. In this case, asymptotic phase changes very little in a small neighborhood near $\mathbf{x_s}$, since $\theta = \omega t$, and only a short time is spent in the neighborhood. A small perturbation in the $V$ direction therefore

takes trajectories to isochrons with similar values of $\theta$, and so has little effect on asymptotic phase. For the integrate-and-fire systems investigated below, spikes are not explicitly modeled. While this may be viewed as an artificial omission leading to $z(\theta_s) \neq 0$, the population dynamics of such systems are of interest because they are in rather common use.

## 3 Phase Response Curves for Specific Models

In this section, we derive or recall analytical approximations to PRCs for multidimensional systems with limit cycles that arise in the four (local and global) codimension one bifurcations (Guckenheimer & Holmes, 1983): these are appropriate to conductance-based models of the form of equations 2.1 and 2.2. We then give PRCs for one-dimensional (linear) integrate-and-fire models. Of these PRC calculations, results for the homoclinic and degenerate Hopf bifurcation are new, while the results for other models, previously derived as referenced in the text, are summarized and recast to display their frequency dependence and for application to population models in what follows.

**3.1 Phase Response Curves Near Codimension One Bifurcations to Periodic Firing.** Bifurcation theory (Guckenheimer & Holmes, 1983) identifies four codimension one bifurcations, which can give birth to a stable limit cycle for generic families of vector fields: a SNIPER bifurcation (saddle-node bifurcation of fixed points on a periodic orbit), a supercritical Hopf bifurcation, a saddle-node bifurcation of limit cycles, and a homoclinic bifurcation (see Figure 2). All four bifurcation types have been identified in specific neuron models as a parameter. Here, the baseline inward current $I^b$, varies; for example, SNIPER bifurcations are found for type I neurons (Ermentrout, 1996) like the Connor model and its two-dimensional Hindmarsh-Rose (HR) reduction (Rose & Hindmarsh, 1989), supercritical Hopf bifurcations may occur for the abstracted FitzHugh-Nagumo (FN) model (Keener & Sneyd, 1998), a saddle-node bifurcation of limit cycles is found for the Hodgkin-Huxley (HH) model (Hodgkin & Huxley, 1952; Rinzel & Miller, 1980), and a homoclinic bifurcation can occur for the Morris-Lecar (ML) model (Rinzel & Ermentrout, 1998).

In this section, we calculate or summarize PRCs for limit cycles arising from all four bifurcations. This is accomplished, where possible, through use of one- and two-dimensional normal form equations. Normal forms are obtained through center manifold reduction of equations 2.1 and 2.2 at the bifurcation, followed by a similarity transformation to put the linear part of the equation into Jordan normal form, and finally by successive near-identity nonlinear coordinate transformations to remove as many terms as possible, a process that preserves the qualitative dynamics of the system (Guckenheimer & Holmes, 1983). To obtain the PRC in terms of the original variables, that is, $\frac{\partial \theta}{\partial V}$, rather than in terms of the normal form variables
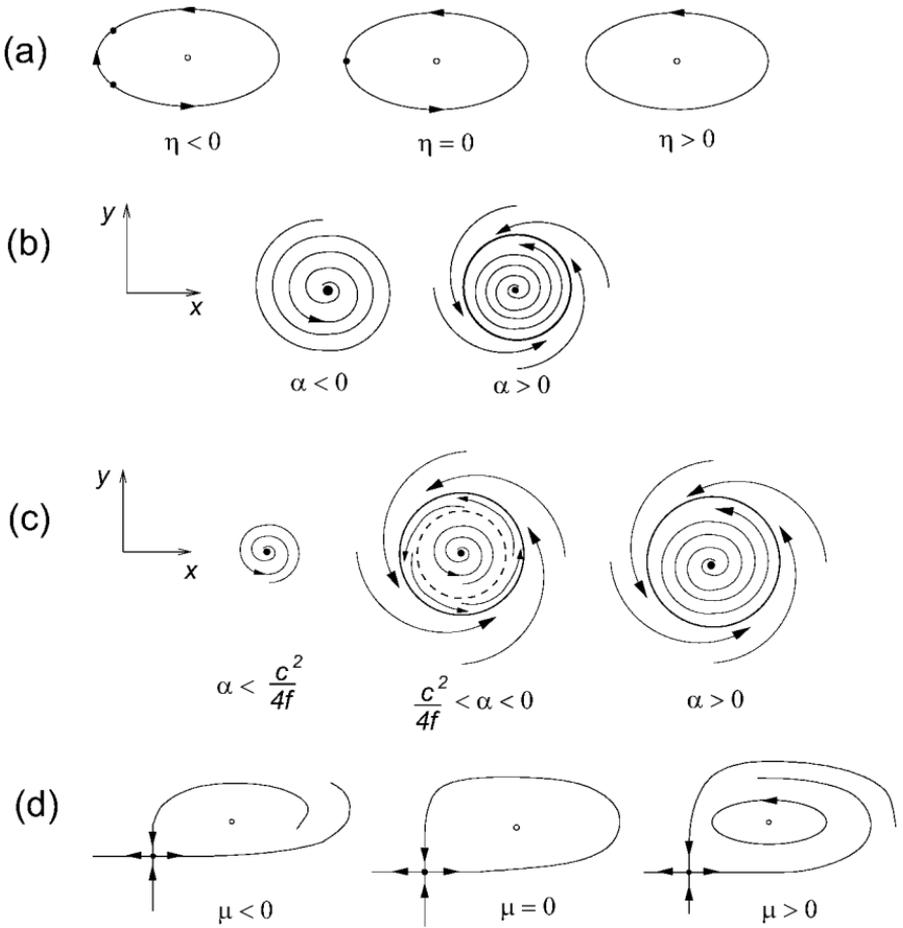
Figure 2: (a) SNIPER bifurcation. Two fixed points die in a saddle-node bifurcation at $\eta = 0$, giving a periodic orbit for $\eta > 0$, assumed to be stable. (b) Supercritical Hopf bifurcation. A fixed point loses stability as $\alpha$ increases through zero, giving a stable periodic orbit (closed curve). (c) Bautin bifurcation. See the text for details. At $\alpha = \frac{c^2}{4f}$ there is a saddle-node bifurcation of periodic orbits. Both a stable (solid closed curve) and unstable (dashed closed curve) periodic orbit exist for $\frac{c^2}{4f} < \alpha < 0$; the unstable periodic orbit dies in a subcritical Hopf bifurcation at $\alpha = 0$. The fixed point is stable (resp., unstable) for $\alpha < 0$ (resp., $\alpha > 0$). (d) Homoclinic bifurcation. A homoclinic orbit exists at $\mu = 0$, giving rise to a stable periodic orbit for $\mu > 0$.

(which we henceforth denote $(x, y)$) with associated PRCs $\frac{\partial \theta}{\partial x}$ and $\frac{\partial \theta}{\partial y}$, it is necessary to undo these coordinate transformations. However, since the normal form coordinate transformations affect only nonlinear terms, we obtain the simple relationship

$$\frac{\partial \theta}{\partial V} = v_x \frac{\partial \theta}{\partial x} + v_y \frac{\partial \theta}{\partial y} + \mathcal{O}(x, y), \tag{3.1}$$

where

$$v_x = \left.\frac{\partial x}{\partial V}\right|_{x=y=0}, \qquad v_y = \left.\frac{\partial y}{\partial V}\right|_{x=y=0}.$$

The remainder term in equation 3.1 is assumed to be small near the bifurcations of relevance and is neglected below. This introduces vanishing error in the Hopf case, in which the bifurcating periodic orbits have arbitrarily small radii; the same is true near SNIPER and homoclinic bifurcations, where periodic orbits spend arbitrarily large fractions of their period near the origin. When using the Bautin normal form, however, we must tacitly assume that the nonzero onset radius of stable bifurcating orbits is small; failure of this assumption for the HH model may contribute to the discrepancy between PRCs derived by analytical and numerical methods (see section 3.3).

Before proceeding, a few notes regarding the normal form equations that we will consider are in order. For the SNIPER bifurcation, we consider the normal form for a saddle-node bifurcation of fixed points, which must be properly embedded globally in order to capture the presence of the periodic orbit (the unstable branch of the center manifold must close up and limit on the saddle node; cf. Figure 2a). For the saddle-node bifurcation of periodic orbits, we appeal to the sequence of bifurcations for type II neurons such as the HH model (Hodgkin & Huxley, 1952), namely, a subcritical Hopf bifurcation in which an unstable periodic orbit branch bifurcates from the rest state, turns around, and gains stability in a saddle-node bifurcation of periodic orbits (Rinzel & Miller, 1980). This sequence is captured by the normal form of the Bautin (degenerate Hopf) bifurcation (Kuznetsov, 1998); cf. Guckenheimer & Holmes, 1983, sec. 7.1). Finally, for the homoclinic bifurcation, we consider only the linearized flow near the fixed point involved in the bifurcation. This is not strictly a normal form, and as for the SNIPER bifurcation, a proper global return interpretation is necessary to produce the periodic orbit.

Near the SNIPER, Hopf, and Bautin local bifurcations, there is a separation of timescales between dynamics along versus dynamics normal to the one- or two-dimensional attracting center manifold containing (or, in the SNIPER case, consisting of) the periodic orbit. In particular, sufficiently close to the bifurcation point, the time required for perturbed solutions to collapse back onto the manifold is negligible compared with the period of

the orbit. This implies that as the bifurcation is approached, the tangent space of any $N-1$ dimensional isochron (computed at its intersection with the periodic orbit) becomes normal to the corresponding tangent space of the center manifold. Thus, sufficiently near these three bifurcations, the only relevant contributions that perturbations make to asymptotic trajectories is by their components along the center manifold, as captured by the above terms $v_x$ and (additionally for the Hopf and Bautin bifurcations) $v_y$. Hence equation 3.1 captures the phase response curve for the full $N$-dimensional system. For the homoclinic global bifurcation, the same conclusion holds, although for a different reason: in this case, there is no low-dimensional center (i.e., locally slow) manifold. However, because the dynamics that asymptotically determine the PRC are linear for the homoclinic bifurcation (unlike the SNIPER, Hopf, and Bautin cases), a PRC valid for full $N$-dimensional systems can still be computed analytically, as described below.

We use the direct method of section 2.2.1 to compute PRCs from the normal form equations. This involves linearizing about the stable periodic orbit, which is appropriate because the perturbations $\Delta V$ to be considered are vanishingly small. The explicit solution of the normal form equations yields $\Delta\theta$, and taking limits, we obtain the PRC (cf. equation 2.8). Without loss of generality, the voltage peak (spike) phase is set at $\theta_s = 0$, and coordinates are defined so that phase increases at a constant rate $\omega$ in the absence of external inputs, as in section 2.1. Analogs of some of the following results have been previously derived by alternative methods, as noted in the text, and we also note that PRCs for relaxation oscillators have been discussed in Izhikevich (2000b). However, unlike the previous work, here we explicitly compute how the PRCs scale with oscillator frequency.

*3.1.1 Saddle Node in a Periodic Orbit (SNIPER).* A SNIPER bifurcation occurs when a saddle-node bifurcation of fixed points takes place on a periodic orbit (see Figure 2a). Following the method of Ermentrout (1996, with details of the calculation), we ignore the direction(s) transverse to the periodic orbit and consider the one-dimensional normal form for a saddle-node bifurcation of fixed points,

$$\dot{x} = \eta + x^2, \tag{3.2}$$

where $x$ may be thought of as local arc length along the periodic orbit. For $\eta > 0$, the solution of equation 3.2 traverses any interval in finite time; as in Ermentrout (1996), the period $T$ of the orbit may be approximated by calculating the total time necessary for the solution to equation 3.2 to go from $x = -\infty$ to $x = +\infty$ and making the solution periodic by resetting $x$ to $-\infty$ every time it fires at $x = \infty$. This gives $T = \frac{\pi}{\sqrt{\eta}}$, hence $\omega = 2\sqrt{\eta}$.

Since equation 3.2 is one-dimensional, Ermentrout (1996) immediately computes

$$\frac{\partial \theta}{\partial x} = \omega \frac{\partial t}{\partial x} = \frac{\omega}{\frac{dx}{dt}}, \tag{3.3}$$

where $\frac{dx}{dt}$ is evaluated on the solution trajectory to equation 3.2. This gives

$$\frac{\partial \theta}{\partial x} = \frac{2}{\omega}[1 - \cos \theta], \tag{3.4}$$

as first derived in Ermentrout (1996), but with explicit $\omega$-dependence displayed here.

Considering a voltage perturbation $\Delta V$, we have

$$\frac{\partial \theta}{\partial V} = z_{SN} = \frac{c_{sn}}{\omega}[1 - \cos \theta], \tag{3.5}$$

where $c_{sn} = 2v_x$ is a model-dependent constant (see equation 3.1). Note that $\frac{\partial \theta}{\partial V}$ is nonnegative or nonpositive according to the sign of $c_{sn}$. Since in type I neuron models (Ermentrout, 1996), a positive voltage perturbation advances phase (and hence causes the neuron to fire sooner), in the following we will generally assume $c_{sn}$ to be positive.

*3.1.2 Generalized and Supercritical Hopf Bifurcations.*   The normal form for the (generalized) Hopf bifurcation (Guckenheimer & Holmes, 1983; Kuznetsov, 1998) is

$$\dot{z} = (\alpha + i\beta)z + (c + id)|z|^2 z + (f + ig)|z|^4 z; \tag{3.6}$$

in polar coordinates, this is

$$\dot{r} = \alpha r + cr^3 + fr^5, \tag{3.7}$$
$$\dot{\phi} = \beta + dr^2 + gr^4. \tag{3.8}$$

We study two cases, always treating $\alpha$ as the bifurcation parameter. In the first case, we assume $c < 0$, yielding a supercritical Hopf bifurcation. For $\alpha < 0$, there is a stable fixed point at the origin that loses stability as $\alpha$ increases through zero, giving birth to a stable periodic orbit with radius $r_{po,H} = \sqrt{-\alpha/c}$ (see Figure 2b). Crucially, $r_{po,H} = 0$ when $\alpha = 0$, so that only terms of cubic order in equations 3.7 and 3.8 are required to capture (unfold) the supercritical Hopf dynamics. Hence we may set $g = f = 0$ for a local analysis.

In the second case, we assume $c > 0$, so that equations 3.7 and 3.8 have a subcritical Hopf bifurcation at $\alpha = 0$, and there is no stable periodic orbit

for any value of $\alpha$ when $g = f = 0$. Hence, we must reintroduce these terms to capture the relevant dynamics. Assuming additionally that $f < 0$, for $\alpha < 0$ there is a stable fixed point at the origin that loses stability in a subcritical Hopf bifurcation at $\alpha = 0$, giving rise to an unstable periodic orbit as $\alpha$ decreases through zero. The branch of unstable periodic orbits turns around at a saddle-node bifurcation of periodic orbits at $\alpha = \frac{c^2}{4f}$; for $\alpha > \frac{c^2}{4f}$ stable periodic solutions exist with radius $r_{po,B} = [\frac{1}{2f}(-c - \sqrt{c^2 - 4\alpha f})]^{1/2}$ (see Figure 2c). This is the generalized Hopf or Bautin bifurcation (identified by the subscript $B$).

In either case, the angular speed is constant on the stable periodic orbit; hence, we set the asymptotic phase $\theta$ equal to the polar angle $\phi$ on the periodic orbit itself. (However, radial level sets of $\phi$ extending off the periodic orbit are not isochrons, since $\dot{\phi}$ varies with $r$.)

We calculate the PRC by linearizing about the attracting periodic orbit $r_{po}$. Letting $r = r_{po} + r'$, we obtain $\dot{r}' = \lambda r' + \mathcal{O}(r'^2)$, where $\lambda$ is the transverse Floquet exponent (eigenvalue) for the stable periodic orbit. In the supercritical Hopf bifurcation, $\lambda = \lambda_H = -2\alpha < 0$ and $r_{po} = r_{po,H}$; in the Bautin, $\lambda = \lambda_B = \frac{1}{f}(c^2 - 4\alpha f + c\sqrt{c^2 - 4\alpha f}) < 0$ and $r_{po} = r_{po,B}$. Here and below, we drop terms of $\mathcal{O}(r'^2)$ because we are concerned with arbitrarily small perturbations (cf. equation 2.8). Solving the linearized radial equation with initial condition $r(0) = r_0$, we obtain

$$r(t) = r_{po} + (r_0 - r_{po})e^{\lambda_j t}, \tag{3.9}$$

with $j = H$ or $B$. Next, integrating equation 3.8 yields

$$\phi(t) = \int_0^t d\phi = \int_0^t [\beta + d(r(s))^2 + g(r(s))^4]ds, \tag{3.10}$$

and taking $\phi(0) = \phi_0$, substituting equation 3.9 in 3.10, letting $t \to \infty$, and dropping terms of $\mathcal{O}(r'^2)$, we obtain the phase $\theta$ associated with the initial condition $(r_0, \phi_0)$:

$$\theta(t) = \phi_0 + (\beta + dr_{po}^2 + gr_{po}^4)t - \frac{2r_{po}(d + 2gr_{po}^2)(r_0 - r_{po})}{\lambda_B}. \tag{3.11}$$

Here we have again used the fact that the polar angle $\phi$ and the phase $\theta$ are identical on the periodic orbit.

Suppose that we start with an initial condition $(x_i, y_i)$ on the periodic orbit, with polar coordinates $(r_{po}, \phi_i)$. As $t \to \infty$, the trajectory with this initial condition has asymptotic phase $\phi_i + (\beta + dr_{po}^2 + gr_{po}^4)t$. Now consider a perturbation $\Delta x$ in the $x$-direction to $(x_f, y_f) = (r_{po} \cos \phi_i + \Delta x, r_{po} \sin \phi_i)$. To lowest order in $\Delta x$, this corresponds, in polar coordinates, to

$$(r_f, \phi_f) = \left(r_{po} + \cos \phi_i \Delta x, \; \phi_i - \frac{\sin \phi_i}{r_{po}} \Delta x\right).$$

Setting $(r_0, \phi_0) = (r_f, \phi_f)$ in equation 3.11 and subtracting the analogous expression with $(r_0, \phi_0) = (r_{po,j}, \phi_i)$, $j = H$ or $B$, we compute the change in asymptotic phase due to this perturbation,

$$\frac{\partial \theta}{\partial x} = -\frac{2dr_{po,j} + 4gr_{po,j}^3}{\lambda_j} \cos\theta - \frac{1}{r_{po,j}} \sin\theta, \tag{3.12}$$

where we have substituted $\theta$ for the polar angle $\phi_i$, again using the fact that the two variables take identical values on the periodic orbit. Similarly, we find

$$\frac{\partial \theta}{\partial y} = -\frac{2dr_{po,j} + 4gr_{po,j}^3}{\lambda_j} \sin\theta + \frac{1}{r_{po,j}} \cos\theta. \tag{3.13}$$

We now express $r_{po,j}$ and $\lambda_j$ in terms of the frequencies of the periodic orbits. In the supercritical Hopf case (recall that we set $g = f = 0$ here), at the bifurcation point, the phase frequency $\omega$ is $\dot{\phi} \overset{\triangle}{=} \omega_H = \beta$, and from equation 3.8, we have $\omega - \omega_H = dr_{po,H}^2$, yielding

$$r_{po,H} = \frac{\sqrt{|\omega - \omega_H|}}{\sqrt{|d|}}. \tag{3.14}$$

Substituting for $r_{po,H}$, we have $\omega - \omega_H = -\alpha d/c$, which together with the expression for $\lambda_H$ gives

$$\lambda_H = \frac{2c}{d}(\omega - \omega_H). \tag{3.15}$$

In the Bautin case, we find that

$$\omega - \omega_{SN} = \left[-\frac{d}{2f} + \frac{gc}{2f^2}\right]\sqrt{c^2 - 4\alpha f} + \frac{g}{4f^2}(c^2 - 4\alpha f), \tag{3.16}$$

where $\omega_{SN}$ is the frequency of the periodic orbit at the saddle-node bifurcation ($\alpha = \frac{c^2}{4f}$). Thus, from equation 3.16,

$$\sqrt{c^2 - 4\alpha f} = k|\omega - \omega_{SN}| + \mathcal{O}(|\omega - \omega_{SN}|^2), \tag{3.17}$$

where $k = |\frac{2f^2}{fd-gc}|$, and we may use the expressions for $r_{po,B}$ and $\lambda_B$ to compute

$$r_{po,B} = \sqrt{\frac{-c}{2f}} + \mathcal{O}(|\omega - \omega_{SN}|), \tag{3.18}$$

$$\lambda_B = \frac{ck}{f}|\omega - \omega_{SN}| + \mathcal{O}(|\omega - \omega_{SN}|^2). \tag{3.19}$$

Next, we substitute these equations 3.14, 3.15, and 3.18, 3.19, for $r_{po}$ and $\lambda$ into equations 3.12 and 3.13. For the supercritical Hopf case, this gives

$$\frac{\partial \theta}{\partial x} = \frac{1}{\sqrt{|\omega - \omega_{SN}|}} \frac{\sqrt{|d|}}{|c|} [d \cos(\theta) + c \sin(\theta)], \qquad (3.20)$$

$$\frac{\partial \theta}{\partial y} = \frac{1}{\sqrt{|\omega - \omega_{SN}|}} \frac{\sqrt{|d|}}{|c|} [d \sin(\theta) - c \cos(\theta)]. \qquad (3.21)$$

In the Bautin case, we get

$$\frac{\partial \theta}{\partial x} = \frac{1}{|\omega - \omega_{SN}|} \left[ -2d\sqrt{\frac{-c}{2f}} - 4g\left(\frac{-c}{2f}\right)^{3/2} \right] \frac{f}{ck} \cos\theta + \mathcal{O}(1), \qquad (3.22)$$

$$\frac{\partial \theta}{\partial y} = \frac{1}{|\omega - \omega_{SN}|} \left[ -2d\sqrt{\frac{-c}{2f}} - 4g\left(\frac{-c}{2f}\right)^{3/2} \right] \frac{f}{ck} \sin\theta + \mathcal{O}(1), \qquad (3.23)$$

where we have explicitly written terms of $\mathcal{O}(|\omega - \omega_{SN}|)^{-1}$, which dominate near the saddle node of periodic orbits. Note that the only term involving the bifurcation parameter $\alpha$ is the prefactor, so that as this parameter is varied, all other terms in equations 3.22 and 3.23 remain constant.

Equipped with equations 3.20 and 3.21, the PRC for a perturbation in the $V$-direction near a supercritical Hopf bifurcation is found from equation 3.1 to be

$$z_H(\theta) = \frac{\partial \theta}{\partial V} = \frac{c_H}{\sqrt{|\omega - \omega_H|}} \sin(\theta - \phi_H), \qquad (3.24)$$

where the constant $c_H = \frac{\sqrt{|d|}}{|c|} \sqrt{(v_x c + v_y d)^2 + (v_x d - v_y c)^2}$ and the phase shift $\phi_H = \tan^{-1}(\frac{v_y c - v_x d}{v_x c + v_y d})$. The form of this PRC was originally presented as equation 2.11 of Ermentrout and Kopell (1984). See that article, as well as section 4 of Ermentrout (1996) and Hoppensteadt and Izhikevich (1997), for earlier, alternative methods and computations for the PRC near supercritical Hopf bifurcation.

For the Bautin bifurcation, we similarly arrive at

$$z_B(\theta) = \frac{\partial \theta}{\partial V} = \frac{c_B}{|\omega - \omega_{SN}|} \sin(\theta - \phi_B). \qquad (3.25)$$

Here $c_B = [-2d\sqrt{\frac{-c}{2f}} - 4g(\frac{-c}{2f})^{3/2}]\frac{f}{ck}\sqrt{v_x^2 + v_y^2}$ is a constant (which can be positive or negative depending on $d$ and $g$), and $\phi_B = \tan^{-1}(\frac{v_x}{v_y})$ is an $\omega$-independent phase shift.

*3.1.3 Homoclinic Bifurcation.* Finally, suppose that the neuron model has
a parameter $\mu$ such that a homoclinic orbit to a hyperbolic saddle point $p$
with real eigenvalues exists at $\mu = 0$. Then there will be a periodic orbit $\gamma$
for, say, $\mu > 0$, but not for $\mu < 0$. Specifically, we assume a single unstable
eigenvalue $\lambda_u$ smaller in magnitude than that of the all stable eigenvalues,
$\lambda_u < |\lambda_{s,j}|$, so that the bifurcating periodic orbit is stable (Guckenheimer &
Holmes, 1983; see Figure 2d).

If parameters are chosen close to the homoclinic bifurcation, solutions
near the periodic orbit spend most of their time near $p$, where the vector
field is dominated by its linearization. This may generically be written in
the diagonal form:

$$\dot{x} = \lambda_u x, \tag{3.26}$$

$$\dot{y}_j = \lambda_{s,j}\, y_j, \;\; j = 1, \ldots, N - 1, \tag{3.27}$$

where the $x$ and $y_j$ axes are tangent to the unstable and a stable manifold of $p$,
respectively, and $\lambda_{s,j} < 0 < \lambda_u$ are the corresponding eigenvalues. For sim-
plicity, we assume here that the segments of the axes shown in Figure 3 are
actually contained in the respective manifolds; this can always be achieved
locally by a smooth coordinate change (Guckenheimer & Holmes, 1983).

We define the box $B = [0, \Delta] \times \cdots \times [0, \Delta]$ that encloses $\gamma$ for the dominant
part of its period, but within which equations 3.26 and 3.27 are still a good
approximation; $\Delta$ is model dependent but fixed for different periodic orbits
occurring as a bifurcation parameter varies within the model. We do not
explicitly model $\gamma$ outside of $B$, but note that the trajectory is reinjected

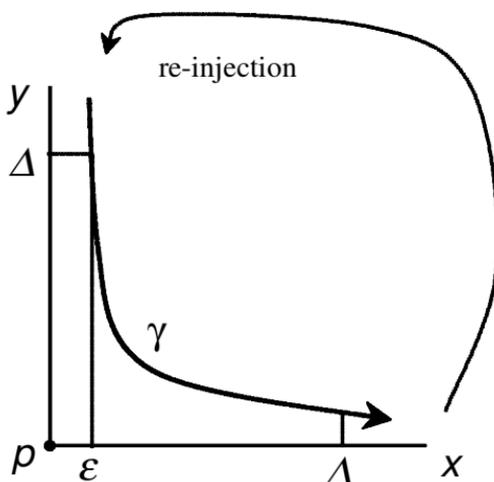

Figure 3: The setup for deriving the PRC for oscillations near a homoclinic
bifurcation, shown (for simplicity) with $N = 2$.

after negligible time (compared with that spent in $B$) at a distance $\epsilon$ from the stable manifold, where $\epsilon$ varies with the bifurcation parameter $\mu$ (see Figure 3). Thus, periodic orbits occurring closer to the bifurcation point correspond to lower values of $\epsilon$ and have larger periods.

We approximate the period $T(\epsilon)$ as the time that the $x$ coordinate of $\gamma$ takes to travel from $\epsilon$ to $\Delta$ under equation 3.26:

$$T(\epsilon) = \frac{1}{\lambda_u} \ln\left(\frac{\Delta}{\epsilon}\right). \tag{3.28}$$

Notice that the $x$-coordinate of $\gamma$ alone determines $T(\epsilon)$, and hence may be thought of as independently measuring the phase of $\gamma$ through its cycle. We set $\theta = 0$ at $x = \epsilon$ and, assuming instantaneous reinjection, $\theta = 2\pi$ at $x = \Delta$. Then $\omega = 2\pi/T(\epsilon)$, and as in equation 3.3,

$$\frac{\partial \theta}{\partial x} = \frac{\omega}{\frac{dx}{dt}} = \frac{\omega}{\lambda_u x(\theta)} = \frac{\omega}{\lambda_u \epsilon} \exp(-\lambda_u \theta/\omega). \tag{3.29}$$

In the final equality, we used the solution to equation 3.26, $x(t) = \epsilon \exp(\lambda_u t)$, with the substitution $t = \theta/\omega$. Since, as remarked above, motion in the $y_j$-directions does not affect the phase of $\gamma$, only components of a perturbation $\Delta V$ along the $x$-axis contribute to the phase response curve; thus, the PRC $z_{HC} = \frac{\partial \theta}{\partial V} = v_x \frac{\partial \theta}{\partial x}$, where $v_x$ is as defined following equation 3.1. Using equation 3.28, $\epsilon = \Delta \exp(-2\pi \lambda_u/\omega)$, which allows us to eliminate $\epsilon$ from equation 3.29:

$$z_{HC}(\theta) = \frac{\partial \theta}{\partial V} = c_{hc}\, \omega \exp\left(\frac{2\pi \lambda_u}{\omega}\right) \exp\left(-\lambda_u \frac{\theta}{\omega}\right), \tag{3.30}$$

where $c_{hc} = \frac{v_x}{\lambda_u \Delta}$ is a model-dependent constant. This is an exponentially decaying function of $\theta$ with maximum

$$z_{\max} = c_{hc}\omega \exp\left(\frac{2\pi \lambda_u}{\omega}\right) \tag{3.31}$$

and minimum

$$z_{\min} = z_{\max} \exp\left(-\frac{2\pi \lambda_u}{\omega}\right) = c_{hc}\omega. \tag{3.32}$$

Here and below we assume $c_{hc} > 0$. $z_{HC}$ is discontinuous at the spike point $\theta_s = 2\pi$, which forces us to take a limit in defining population-averaged firing rates below but does not otherwise affect the following analysis.

**3.2 One-Dimensional Neuron Models.** Generalized integrate-and-fire models have the form

$$\dot{V} = F(V) + G(V, t), \tag{3.33}$$

where $V(t)$ is constrained to lie between a reset voltage $V_r$ and a threshold $V_{th}$, and the following reset dynamics are externally imposed: if $V(t)$ crosses $V_{th}$ from below, a spike occurs, and $V(t)$ is reset to $V_r$. Here, nothing is lost in transforming to the single phase equation, 2.6; in particular, the error term of equation 2.5 does not apply. In fact, as noted in Ermentrout (1981), the crucial quantity $\frac{\partial \theta}{\partial V}$ can be found directly from equation 3.33 with $G(V, t) \equiv 0$:

$$z(\theta) = \frac{\partial \theta}{\partial V} = \omega \frac{\partial t}{\partial V} = \frac{\omega}{F(V(\theta))}, \tag{3.34}$$

where we recall that $\theta$ is defined such that $\dot{\theta} = \omega$. In the next two subsections, we compute phase response curves for two simple integrate-and-fire models.

*3.2.1 Integrate-and-Fire Neuron.* We first consider the simplest possible integrate-and-fire (IF) model:

$$C\dot{V} = (I_b + I(t)); \quad V_r = 0, \quad V_{th} = 1, \tag{3.35}$$

where $I_b$ is the baseline current, $C$ is membrane capacitance, and $G(V, t) = I(t)$. Hereafter we set $C = 1$ for the IF model. The angular frequency of a baseline ($I(t) = 0$) oscillation is $\omega = 2\pi I_b$, and equation 3.34 gives

$$z_{IF}(\theta) = \frac{\omega}{F(V(\theta))} = \frac{\omega}{I_b} \equiv 2\pi. \tag{3.36}$$

Thus, the IF PRC is constant in $\theta$ and frequency independent.

*3.2.2 Leaky IF Neuron.* Next, we consider the leaky integrate and fire (LIF) model:

$$C\dot{V} = (I_b + g_L(V_L - V) + I(t)); \quad V_r = 0, \quad V_{th} = 1 < V_L + \frac{I_b}{g_L}, \tag{3.37}$$

where $I_b$ is the baseline current, $g_L > 0$ and $V_L$ are the leak conductance and reversal potential, $C$ is the capacitance, and $G(V, t) = I(t)$. As above, we also set $C = 1$ for this model. We assume $I_b \geq g_L(1 - V_L)$ so that when $I(t) = 0$, the neuron fires periodically with frequency

$$\omega = 2\pi g_L \left[ \ln \left( \frac{I_b + g_L V_L}{I_b + g_L V_L - g_L} \right) \right]^{-1}. \tag{3.38}$$

This expression shows how $I_b$ enters as a bifurcation parameter, with $I_b = g_L(1 - V_L)$ corresponding to the bifurcation point at which $\omega = 0$.

Solving equation 3.37 for $V(t)$ with initial condition $V(0) = V_r = 0$, and then using $\theta = \omega t$ and equation 3.34, gives

$$z_{LIF}(\theta) = \frac{\omega}{g_L}\left(1 - \exp\left(-\frac{2\pi g_L}{\omega}\right)\right)\exp\left(\frac{g_L\theta}{\omega}\right), \tag{3.39}$$

equivalent to formulas previously derived in van Vreeswijk et al. (1994) and Lewis and Rinzel (2003). Thus, the PRC for the LIF model is an exponentially increasing function of $\theta$, with a maximum that decreases with $\omega$:

$$z_{\max}(\omega) = \frac{\omega}{g_L}\left(\exp\left(\frac{2\pi g_L}{\omega}\right) - 1\right), \tag{3.40}$$

and minimum

$$z_{\min}(\omega) = z_{\max}\exp\left(-\frac{2\pi g_L}{\omega}\right) = \frac{\omega}{g_L}(1 - e^{-2\pi g_L/\omega}). \tag{3.41}$$

Recall that the PRC near a homoclinic bifurcation is also an exponential function but with opposite slope: this is because both the essential dynamics near a homoclinic bifurcation and the LIF dynamics are linear, while the trajectories accelerate following spikes in the homoclinic case and decelerate in the LIF.

This is our final analytical PRC calculation; we summarize the results derived above in Table 1 and Figure 4.

Table 1: Phase Response Curves for the Different Neuron Models.

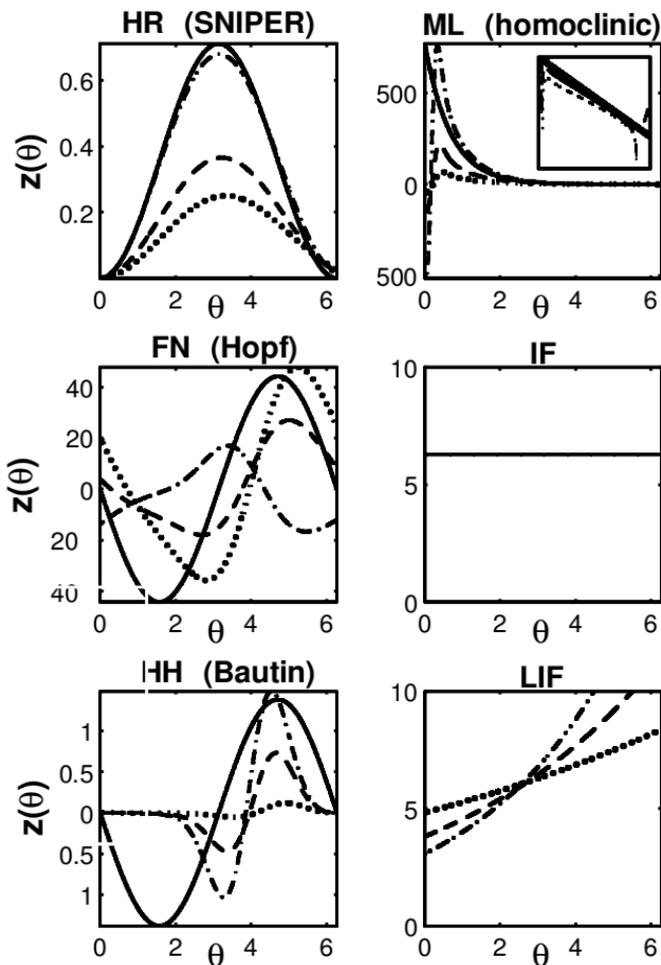| Bifurcation | $z(\theta)$ | $z_{\max}$ | $z_{\min}$ |
|---|---|---|---|
| SNIPER | $\frac{c_{sn}}{\omega}[1 - \cos(\theta)]$ | $\frac{2c_{sn}}{\omega}$ | $0$ |
| Hopf | $\frac{c_H}{\sqrt{|\omega - \omega_H|}}[\sin(\theta - \phi_H)]$ | $\frac{c_H}{\sqrt{|\omega - \omega_H|}}$ | $-\frac{c_H}{\sqrt{|\omega - \omega_H|}}$ |
| Bautin | $\frac{|c_B|}{|\omega - \omega_{SN}|}[\sin(\theta - \phi_B)] + \mathcal{O}(1)$ | $\frac{|c_B|}{|\omega - \omega_{SN}|} + \mathcal{O}(1)$ | $-\frac{|c_B|}{|\omega - \omega_{SN}|} + \mathcal{O}(1)$ |
| Homoclinic | $c_{hc}\,\omega\exp\left(\frac{2\pi\lambda_u}{\omega}\right)\exp\left(-\lambda_u\theta/\omega\right)$ | $c_{hc}\omega\exp\left(\frac{2\pi\lambda_u}{\omega}\right)$ | $c_{hc}\omega$ |
| IF | $2\pi$ | $2\pi$ | $2\pi$ |
| LIF | $\frac{\omega}{g_L}\left(1 - e^{-2\pi g_L/\omega}\right)e^{g_L\theta/\omega}$ | $\frac{\omega}{g_L}\left(e^{2\pi g_L/\omega} - 1\right)$ | $\frac{\omega}{g_L}(1 - e^{-2\pi g_L/\omega})$ |

Figure 4: PRCs for the various neuron models, from the formulas of section 3 and numerically computed using XPP (Ermentrout, 2002), all with $\theta_s = 0$. The relevant bifurcations are noted where applicable. Dot-dashed, dashed, and dotted curves for each model correspond to increasing frequencies, respectively: HR: $\omega = 0.0102, 0.0201, 0.0316$ rad/msec (corresp. 1.62, 3.20, 5.03 Hz); FN: $\omega = 0.204, 0.212, 0.214$ (corresp. 32.5, 33.7, 34.1 Hz); HH: $\omega = 0.339, 0.355, 0.525$ rad/msec (corresp. 54.2, 56.5, 83.6 Hz); ML: $\omega = 0.0572, 0.0664, 0.0802$ rad/msec (corresp. 9.10, 10.6, 12.8 Hz); IF: (any frequency); LIF: $\omega = 0.419, 0.628, 1.26$ rad/msec (corresp. 66.7, 100, 200 Hz). For the LIF model, $g_L = 0.110$. Normal forms 3.5, 3.24, 3.25, and 3.30 for the PRCs closest to bifurcation shown solid (scale factors $c_i$ fit by least squares); the IF and LIF PRCs are exact. PRC magnitudes decrease with $\omega$ for the HR, HH, ML, and LIF models; are constant for the IF model; and increase with $\omega$ for the FN model. The phase shifts $\phi_H$ and $\phi_B$ are chosen as $\pi$ (yielding $z(\theta_s) = 0$; see section 2.3). The inset to the ML plot displays the same information on a log scale, demonstrating exponential decay.
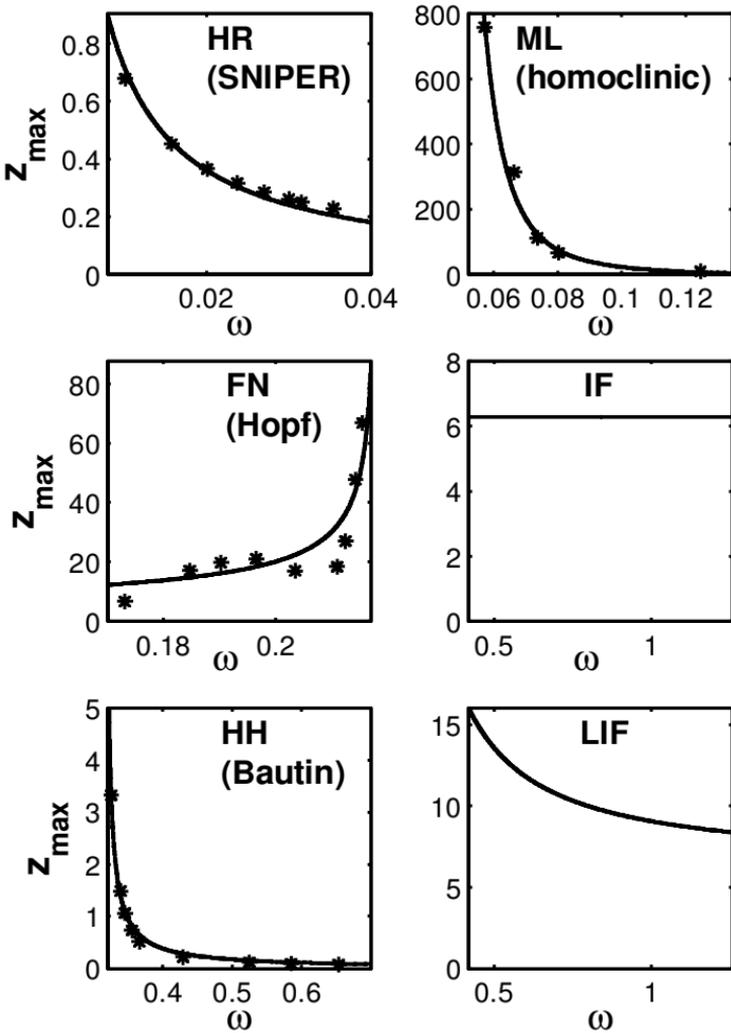
Figure 5: Scaling of $z_{max}$ with $\omega$ for the various neuron models (and hence scaling of the population response $FL^d_{max} - FL^b$ with $\omega$; see section 4.2). Asterisks are numerical values from the PRCs of the full HR, FN, HH, and ML models, and curves show predictions of the normal forms 3.5, 3.25, 3.24, and 3.30 with least-squares fits (of PRC maxima) for scale factors. Results for the IF and LIF models are exact.

**3.3 Accuracy of the Analytical PRCs.** The range of parameters over which the PRCs of the full neuron models are well approximated by the analytical expressions derived above varies from model to model. One overall limitation, noted in Izhikevich (2000a), is that normal form calculations for the Bautin and supercritical Hopf bifurcation ignore the relaxation nature of the dynamics of typical neural oscillators. However, the analytical PRCs— equations 3.5, 3.24, 3.25, and 3.30—are qualitatively, and in many cases quantitatively, correct. Figure 4 compares these formulas with PRCs calculated using XPP (Ermentrout, 2002) for the HR, FN, HH, and ML models near the relevant bifurcations (PRCs for the integrate-and-fire models are exact). The companion Figure 5 demonstrates the scaling of PRC maxima with baseline frequency, which is also correctly predicted by the normal form analysis. Frequencies $\omega$ were varied by changing the bifurcation parameter: baseline inward current $I^b$. Here and elsewhere, the neural models are as given in Rose and Hindmarsh (1989), Murray (2002), Hodgkin and Huxley (1952), and Rinzel and Ermentrout (1989). All parameter values used here are reproduced along with the equations in appendix C. Finally, looking forward to the next section, we note that the analytical PRCs derived here will correctly predict key qualitative aspects of population responses to stimuli.

## 4 Probabilistic Analysis of Firing Rates

**4.1 A Phase Density Equation.** We now describe how time-dependent firing rates in response to external stimuli emerge from averages of oscillator population dynamics with appropriate initial conditions. Let $\rho(\theta, t)$ denote the probability density of solutions of equation 2.7. Thus, $\rho(\theta, t)d\theta$ is the probability that a neuron's phase in an arbitrary trial lies in the interval $[\theta, \theta + d\theta]$ at time $t$. This density evolves via the advection equation:

$$\frac{\partial \rho(\theta, t)}{\partial t} = -\frac{\partial}{\partial \theta}[v(\theta, t) \, \rho(\theta, t)]. \tag{4.1}$$

Boundary conditions are periodic in the probability flux: $v(0, t) \rho(0, t) = \lim_{\psi \to 2\pi} v(\psi, t)\rho(\psi, t)$, which reduces to $\rho(0, t) = \rho(2\pi, t)$ for smooth phase response curves $z$. A related phase density approach is used in Tass (1999) and Ritt (2003), and we first derived the solution in Brown et al. (2003b). In the presence of noise, there is an additional diffusion term in equation 4.1 (Stein, 1965; Tass, 1999; Brown et al., 2003b).

Multiple trials in which stimuli are not keyed to oscillator states may be modeled by averaging solutions of the linear PDE equation 4.1 over suitably distributed initial conditions; since (unmodeled) noise and variable and/or drifting frequencies tend to distribute phases uniformly in the absence of stimuli, we set $\rho_0 \equiv 1/2\pi$. Histograms of firing times may then be extracted by noting that firing probabilities for arbitrary cells at time $t$ are equal to the passage rate of the probability density through the spike phase, that is, the

probability flux

$$FL(t) \stackrel{\triangle}{=} \lim_{\psi \to \theta_s^-} v(\psi, t)\, \rho(\psi, t) = \lim_{\psi \to \theta_s^-} [\omega + z(\psi)I(t)]\, \rho(\psi, t) . \tag{4.2}$$

The limit from below allows for discontinuities in $z(\theta)$ (as in the homoclinic and LIF PRCs), since the relevant quantity is flux across the spike threshold from lower values of $V$ and hence from lower values of $\theta$. If the PRC $z(\theta)$ and hence $\rho(\theta, t)$ are continuous at $\theta_s$, equation 4.2 simply becomes $FL(t) = [\omega + z(\theta_s)I(t)]\, \rho(\theta_s, t)$.

We emphasize that expression 4.2 equally describes the average firing rate of an entire uncoupled population on a single trial or the average firing rate of single neurons drawn from such a population over many sequential trials, as in Herrmann and Gerstner (2001), or a combination of both.

**4.2 Patterns of Firing Probabilities and Conditions for Refractory Periods.** Equation 4.1 can be explicitly solved for piecewise constant stimuli of duration $d = t_2 - t_1$: $I(t) = \bar{I}$ for $t_1 \leq t \leq t_2$ and $I(t) = 0$ otherwise. (Here and elsewhere, we assume $\bar{I} > 0$ unless explicitly noted.) Specifically, the method of characteristics (Whitham, 1974; pp. 97–100 of Evans, 1998) yields

$$\rho(\theta, t) = \rho_0(\Theta_{\theta,t}(0)) \exp\left(-\int_0^t \frac{\partial}{\partial \theta} v(\Theta_{\theta,t}(t'), t')dt'\right)$$

$$= \frac{1}{2\pi} \exp\left(-\bar{I}\int_{t_1}^{\tilde{t}_2} z'[\Theta_{\theta,t}(s)]ds\right), \tag{4.3}$$

where $t \geq t_1$, $\tilde{t}_2 = \min(t, t_2)$ and we take the initial condition $\rho_0 = \rho(\theta, 0) = 1/2\pi$. Here, $\Theta_{\theta,t}(s)$ lies on the characteristic curve given by

$$\frac{d}{ds}\Theta_{\theta,t}(s) = v(\Theta_{\theta,t}(s), s), \tag{4.4}$$

with end point condition $\Theta_{\theta,t}(t) = \theta$. When $\Theta_{\theta,t}(s)$ coincides with a discontinuity in $z$, the integrands in equation 4.3 are not defined, and we must appeal to the continuity of probability flux or, equivalently, to the following change of variables.

We now simplify expression 4.3. Using the fact that $v(\Theta_{\theta,t}(s), s) = \omega + \bar{I}z(\Theta_{\theta,t}(s))$ for $t_1 \leq s \leq t_2$, and changing variables from $s$ to $\Theta_{\theta,t}(s)$,

$$\int_{t_1}^{\tilde{t}_2} z'[\Theta_{\theta,t}(s)]ds = \int_{\Theta_{\theta,t}(t_1)}^{\Theta_{\theta,t}(\tilde{t}_2)} \frac{z'[\Theta_{\theta,t}(s)]}{\omega + \bar{I}z(\Theta_{\theta,t}(s))} d\Theta_{\theta,t}(s)$$

$$= \frac{1}{\bar{I}} \ln\left[\frac{\omega + \bar{I}z(\Theta_{\theta,t}(\tilde{t}_2))}{\omega + \bar{I}z(\Theta_{\theta,t}(t_1))}\right], \tag{4.5}$$

so that

$$\rho(\theta, t) = \frac{1}{2\pi} \left[ \frac{\omega + \bar{I}z(\Theta_{\theta,t}(t_1))}{\omega + \bar{I}z(\Theta_{\theta,t}(\tilde{t}_2))} \right]. \tag{4.6}$$

This expression is valid everywhere it is defined. To obtain the terms in equation 4.6, we integrate equation 4.4 backward in time from the final condition at $s = t$ until $s = t_1$ or $s = \tilde{t}_2$; this may be done analytically for the normal form PRCs of section 3 or numerically for PRCs from full neuron models. The integration yields the PRC-independent expression

$$\Theta_{\theta,t}(\tilde{t}_2) = \theta - \omega(t - \tilde{t}_2) \tag{4.7}$$

for all neuron models, while $\Theta_{\theta,t}(t_1)$ is model dependent via the PRC.

Note that while the stimulus is on (i.e., $t_1 \leq t \leq t_2$), $\tilde{t}_2 = t$ so that $\Theta_{\theta,t}(\tilde{t}_2) = \theta$. After the stimulus turns off, $v(\theta, t)$ is independent of $\theta$, and $\rho$ is constant along curves with constant $\theta - \omega t$. Thus, for $t > t_2$, $\rho(\theta, t)$ is simply a traveling wave rotating with frequency $\omega$, with $\rho(\theta, t_2)$ determining the phase density.

From the definition 4.2, we have:

$$FL(t) = \lim_{\psi \to \theta_s} \frac{\omega + z(\psi)I(t)}{2\pi} \left[ \frac{\omega + \bar{I}z(\Theta_{\psi,t}(t_1))}{\omega + \bar{I}z(\Theta_{\psi,t}(\tilde{t}_2))} \right]. \tag{4.8}$$

Figure 6 shows examples of $FL(t)$ for the various neuron models, computed via equation 4.8 with both numerically and analytically derived PRCs $z$, as well as as via numerical simulations of the full neuron models. The phase reduction 4.8 gives qualitative, and in some cases precise, matches to the full numerical data. We recall that the accuracy of phase reductions from full neuron models improves with weaker stimuli $\bar{I}$ and that the analytical PRCs better approximate their numerical counterparts as the bifurcation point is approached (i.e., as $I_b$ is varied).

Note that if $\lim_{\psi \to \theta_s} z(\psi) = 0$, $I(t)$ does not directly enter equation 4.8, so $FL(t)$ depends only on variations in $\rho$ resulting from the stimulus. However, **(I) if $\lim_{\psi \to \theta_s} z(\psi) \neq 0$, the firing probability $FL(t)$ jumps at stimulus onset and offset**. See Figure 6, and recall that we set $\theta_s = 0$. This is our first main result.

Some comments on the limit in equation 4.8 are appropriate. Since for all neuron models, we always assume that $v(\theta)$ is positive and bounded and is defined except at isolated point(s), $\Theta_{\psi,t}(s)$ is a continuous function of $\psi$, $s$ and $t$. Nevertheless, as $\Theta_{\psi,t}(t_1)$ and $\Theta_{\psi,t}(\tilde{t}_2)$ pass through $\theta_s$ as $t$ advances, discontinuities in $z(\cdot)$ give discontinuities in $FL(t)$, but the limit in equation 4.8 ensures that $FL(t)$ is always defined. As remarked above, if the PRC $z(\cdot)$ is a continuous function, then $\lim_{\psi \to \theta_s} z(\psi) = z(\theta_s)$ and taking the limit is unnecessary.

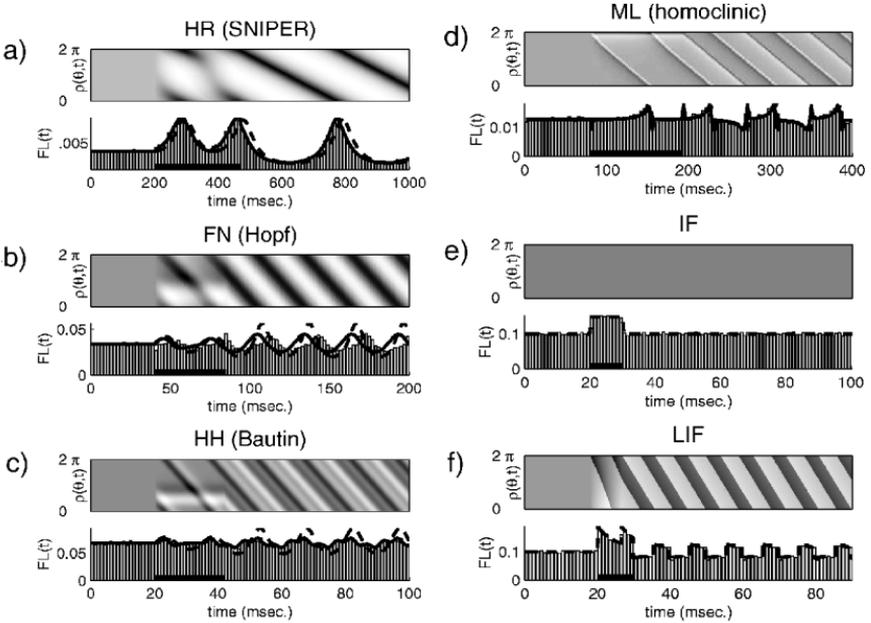Figure 6: (a–f) Phase density $\rho(\theta, t)$ in gray scale (darker corresponding to higher values) (top) and firing probability $FL(t)$ in msec$^{-1}$ (bottom) for stimuli of length $3/2 \times P$ (indicated by black horizontal bars), from equations 4.6 and 4.8 via the method of characteristics. Dashed curves indicate $FL(t)$ from the normal form PRCs of equations 3.5, 3.24, 3.25, 3.30, 3.36, and 3.39; solid curves from numerical PRCs computed via XPP. Baseline frequencies and values of $\bar{I}$ for HR, FN, HH, ML, IF, and LIF models are (0.0201, 0.212, 0.429, 0.08, 0.628, 0.628) rad/msec (corresp. 3.20, 33.7, 68.3, 12.7, 100, 100 Hz) and (0.1, 0.0015, 0.25, 0.0005, 0.05, 0.05) $\mu$A/cm$^2$, respectively. The vertical bars are PSTHs, numerically computed using the full conductance-based equations (see appendix C) using 10,000 initial conditions, with $I_b$ set to match frequencies of the corresponding phase models. Initial conditions generated by evolving the full equations for a (uniformly distributed) random fraction of their period, from a fixed starting point. Note that $FL(t)$ jumps discontinuously at stimulus onset and offset for the IF and LIF models, since for these models, $z(\theta_s) \neq 0$ (point I in text). Also, during stimulus, $FL(t)$ does not dip below the baseline value $\frac{\omega}{2\pi}$ for the HR, IF, and LIF models, because $z_{\min} \approx 0$ in these cases (point V).

While the stimulus is on, solutions to equation 4.4 are periodic with period

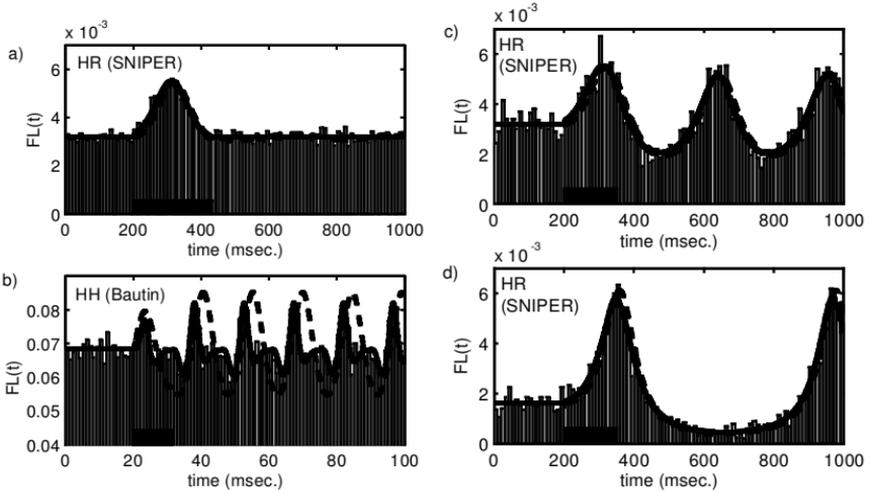$$P = \int_0^{2\pi} \frac{d\theta}{\omega + \bar{I}z(\theta)} \tag{4.9}$$

Figure 7: (a–d) Firing probabilities $FL(t)$ for the HH and HR models, with stimulus characteristics chosen to illustrate the points in the text. Dashed and solid curves and vertical bars denote data obtained as in Figure 6. (a) A stimulus ($\bar{I} = 0.04\ \mu A/cm^2$) of length exactly $P = 232.50$ msec (indicated by the horizontal black bar) for the HR model ($\omega = 0.0201$ rad/msec) leaves no trace (point II). (b) A stimulus ($\bar{I} = 0.25\ \mu A/cm^2$) of duration $d_{max} = 11.46$ msec for the HH model ($\omega = 0.429$ rad/msec) yields maximum response after the stimulus has switched off (because $z_{min} < 0$) but for the HR model (d) ($\omega = 0.0102$ rad/msec) with stimulus duration $d_{max} = 152.01$ msec, the peak in $FL(t)$ is achieved at $t_2$ (because $z_{min} \approx 0$), (points III, IVa). Plots $c$ and $d$ illustrate point VI: the stimulus in $c$ is identical to that of $d$, but the slower HR population $d$ ($\omega = 0.0102$ versus $0.0201$ rad/msec) displays the greatest response.

(independent of the end point condition). Thus, equation 4.6 implies that $\rho(\theta, t)$ must also be $P$-periodic, so that the distribution returns to $\rho(\theta, t_1) \equiv \frac{1}{2\pi}$ every $P$ time units: that is, $\rho(\theta, t_1 + kP) \equiv \frac{1}{2\pi}$ for integers $k$. If the stimulus is turned off after duration $d = t_2 - t_1 = kP$, this flat density therefore persists (recall that $\rho$ evolves as a traveling wave), giving our second result: **(II) for stimulus durations that are multiples of $P$, poststimulus firing probabilities $FL(t)$ return to the constant value $\frac{\omega}{2\pi}$.** This is illustrated in Figure 7a and corresponds to the absence of poststimulus refractory periods and ringing, and is related to the black holes discussed in Tass (1999). Figures 6 and 7 also illustrate the periodic regimes both during and after the stimulus.

When the stimulus duration $d$ is not a multiple of $P$ (and provided $z(\theta)$ is not constant), $\rho(\theta, t_2)$ has at least one peak exceeding $1/2\pi$ and at least one valley less than $1/2\pi$ (see phase density plots of Figure 6). Let the largest and smallest possible $\rho$ values be $\rho_{max}$ and $\rho_{min}$, respectively. Equation 4.6

then gives

$$\rho_{\max} = \frac{1}{2\pi}\left[\frac{\omega + \bar{I}z_{\max}}{\omega + \bar{I}z_{\min}}\right]; \quad \rho_{\min} = \frac{1}{2\pi}\left[\frac{\omega + \bar{I}z_{\min}}{\omega + \bar{I}z_{\max}}\right], \tag{4.10}$$

where $z_{\min} \equiv z(\theta_{\min})$ and $z_{\max} \equiv z(\theta_{\max})$ are the global extrema of the PRC; note the relationship $\rho_{\min}\rho_{\max} = 1/4\pi^2$. Recalling that $\Theta_{\theta,t}(\tilde{t}_2) = \theta$ during the stimulus, comparing equations 4.10 and 4.6 shows that $\rho_{\max}$ occurs at $\theta_{\min}$ and $\rho_{\min}$ at $\theta_{\max}$. When it exists, the stimulus duration $d_{\max}$ (resp., $d_{\min}$) for which a distribution with peak $\rho_{\max}$ (resp., valley $\rho_{\min}$) occurs is essentially obtained by requiring (ignoring the limits required for discontinuous PRCs) that a characteristic curve passes through $\theta_{\max}$ (resp., $\theta_{\min}$) at $t_1$ and through $\theta_{\min}$ (resp., $\theta_{\max}$) at time $t_2$. Thus, **(III) for stimulus durations $d_{\max}$ (resp., $d_{\min}$), poststimulus firing probabilities $FL(t)$ exhibit their maximal deviation above (resp., below) the baseline rate $\frac{\omega}{2\pi}$.** These deviations may or not be exceeded during the stimulus itself. (See Figure 7 for examples and Figure 6 for the evolution of phase density during a prolonged stimulus; in particular, note that while $d_{\max}$ is not strictly defined for the LIF model, shorter stimuli (of arbitrarily small duration) always give higher peaks.)

We now determine whether maximal peaks and minimal valleys in firing rates occur during or after stimulus for the various neuron types. Again using $\Theta_{\psi,t}(\tilde{t}_2) = \psi$ during the stimulus, equation 4.8 yields

$$FL^d(t) = \lim_{\psi \to \theta_s} \frac{\omega + z(\psi)\bar{I}}{2\pi}\left[\frac{\omega + \bar{I}z(\Theta_{\psi,t}(t_1))}{\omega + \bar{I}z(\psi)}\right]$$

$$= \lim_{\psi \to \theta_s} \frac{1}{2\pi}[\omega + \bar{I}z(\Theta_{\psi,t}(t_1))], \quad t_1 < t \le t_2. \tag{4.11}$$

The superscript on $FL^d(t)$ denotes "during" the stimulus, emphasizing that this expression is valid only for $t_1 < t \le t_2$. After the stimulus has turned off, a different special case of equation 4.8 is valid:

$$FL^a(t) = \lim_{\psi \to \theta_s} \frac{\omega}{2\pi}\left[\frac{\omega + \bar{I}z(\Theta_{\psi,t}(t_1))}{\omega + \bar{I}z(\Theta_{\psi,t}(t_2))}\right], \quad t > t_2. \tag{4.12}$$

Here the superscript on $FL^a(t)$ denotes "after" the stimulus. We now use these expressions to write the maximum and minimum possible firing rates during and after the stimulus:

$$FL^d_{\max} = \frac{1}{2\pi}[\omega + \bar{I}z_{\max}] \tag{4.13}$$

$$FL^a_{\max} = \frac{\omega}{2\pi}\left[\frac{\omega + \bar{I}z_{\max}}{\omega + \bar{I}z_{\min}}\right] \tag{4.14}$$

$$FL_{\min}^d = \frac{1}{2\pi} \left[ \omega + \bar{I} z_{\min} \right] \tag{4.15}$$

$$FL_{\min}^a = \frac{\omega}{2\pi} \left[ \frac{\omega + \bar{I} z_{\min}}{\omega + \bar{I} z_{\max}} \right]. \tag{4.16}$$

From equations 4.13 through 4.16, we have

$$FL_{\max}^d - FL_{\max}^a = \frac{1}{2\pi} \left[ \frac{\omega + \bar{I} z_{\max}}{\omega + \bar{I} z_{\min}} \right] \bar{I} z_{\min}, \tag{4.17}$$

$$FL_{\min}^d - FL_{\min}^a = \frac{1}{2\pi} \left[ \frac{\omega + \bar{I} z_{\min}}{\omega + \bar{I} z_{\max}} \right] \bar{I} z_{\max}. \tag{4.18}$$

Since we restrict to the case where $v(\theta, t) > 0$ (i.e., there are no fixed points for the phase flow), the terms in the brackets of the preceding equations are always positive. This implies, for $\bar{I} > 0$,

$$FL_{\max}^a \geq FL_{\max}^d \text{ if and only if } z_{\min} \leq 0, \tag{4.19}$$

$$FL_{\max}^a \leq FL_{\max}^d \text{ if and only if } z_{\min} \geq 0, \tag{4.20}$$

$$FL_{\min}^a \leq FL_{\min}^d \text{ if and only if } z_{\max} \geq 0, \tag{4.21}$$

$$FL_{\min}^a \geq FL_{\min}^d \text{ if and only if } z_{\max} \leq 0, \tag{4.22}$$

where the "equals" cases of the inequalities require $z_{\max} = 0$ or $z_{\min} = 0$. In other words, **(IVa) for the specific stimulus durations that elicit maximal peaks in firing rates, these maximal peaks occur during the stimulus if** $z_{\min} \geq 0$ **but after the stimulus switches off if** $z_{\min} \leq 0$**; (IVb) for the specific (possibly different) stimulus durations that elicit minimal firing rate dips, these minimal dips occur during the stimulus if** $z_{\max} \leq 0$ **but after the stimulus switches off if** $z_{\max} \geq 0$**.** We recall that $z_{\min} < 0$ is a defining condition for type II neurons (Ermentrout, 1996). The poststimulus maximum (resp. minimum) firing rates are obtained as the peak (resp. valley) of the distribution $\rho(\theta, t)$ passes through $\theta_s$. As Figure 7b shows, the delay from stimulus offset can be significant for typical neuron models.

Defining the baseline rate valid for $t < t_1$,

$$FL^b(t) \equiv \frac{\omega}{2\pi}, \tag{4.23}$$

equation 4.15 shows that $FL_{\min}^d \geq FL^b$ if and only if $z_{\min} \geq 0$. Thus, **(V) if** $z_{\min} \geq 0$**, the firing rate does not dip below baseline values until (possibly) after the stimulus switches off.** Table 2 summarizes the above results for the neuron models studied here.

Table 2: Predictions Using the Numerical PRCs of Figure 4.

| Neuron Model | Response "Jumps" With Stimulus? (point I) | Maximum Response *After* Stimulus and Depressed Firing *During* Stimulus? (points IV and V) |
|:---:|:---:|:---:|
| HR | No | No |
| HH | No | Yes |
| FN | Yes | Yes |
| ML | Yes | No |
| IF | Yes | No |
| LIF | Yes | No |

Note: The conclusions follow from the limiting value of $z(\theta_s)$ (point I in text), and the value of the PRC minimum $z_{min}$ (points IVa and V).

We conclude this section by noting that Fourier transformation of the analog of equation 4.1 in the presence of noise shows that $FL(t)$ decays at exponential or faster rates due to noise and averaging over distributions of neuron frequencies (cf. Tass, 1999; Brown et al., 2003b). For mildly noisy or heterogeneous systems, the results I through V remain qualitatively similar but are smeared; for example, $\rho(\theta, t)$ is no longer time periodic during or after the stimulus, but approaches a generally nonuniform equilibrium state via damped oscillations.

**4.3 Frequency Scaling of Response Magnitudes.** We now determine how the maximum and minimum deviations from baseline firing rates depend on the baseline (prestimulus) firing rate of the neural population. Following the discussion of the previous section, we separately compute the scaling of maximal (minimal) responses that are possible *during* stimulus and the scaling of maximal (minimal) responses that are possible *after* stimuli switch off. Equations 4.13 through 4.16 and 4.23 yield

$$FL_{max}^d - FL^b = \frac{1}{2\pi}[\bar{I}z_{max}] \tag{4.24}$$

$$FL_{min}^d - FL^b = \frac{1}{2\pi}[\bar{I}z_{min}] \tag{4.25}$$

$$FL_{max}^a - FL^b = \frac{\omega}{2\pi}\left[\frac{\bar{I}(z_{max} - z_{min})}{\omega + \bar{I}z_{min}}\right] \tag{4.26}$$

$$FL_{min}^a - FL^b = \frac{\omega}{2\pi}\left[\frac{\bar{I}(z_{min} - z_{max})}{\omega + \bar{I}z_{max}}\right]. \tag{4.27}$$

These expressions provide one set of measures of the sensitivity of population-level response at different baseline firing rates. Additionally, taking

ratios with the prestimulus firing rate (e.g., finding $\frac{FL^d_{max}-FL^b}{FL^b}$) determines the size of deviations relative to baseline activity. We use the information summarized in Table 1 to compile these measures for all neuron models in Tables 3 through 6. Note that in these tables, "moving away from the bifurcation" means varying parameters so that the frequency varies away from its value at the onset of firing, namely, $\omega = 0$ for the SNIPER and homoclinic bifurcations and IF and LIF models, $\omega_H$ for the supercritical Hopf bifurcation, and $\omega_{SN}$ for the Bautin bifurcation. The scaling of $FL^d_{max} - FL^b$, as an example, is confirmed by Figure 5. In summary, **(VI) different neural models and bifurcations imply different scalings of maximal response magnitude with frequency.**

Most measures of population firing rate responses increase for frequencies closer to the bifurcation point (see Tables 3–6). If these models are parameterized so that frequency increases as the bifurcation parameter $I_b$ increases through the bifurcation point, this means that populations at lower frequencies tend to display greater responses (see Figure 5 for examples). This effect is explored in the next section.

Table 3: Scaling of Deviations in Firing Rate During Stimulus $FL^d_{max} - FL^b$ for the Different Neuron Models.

| Bifurcation | $FL^d_{max} - FL^b$ | Lowest Order Scaling Near Bifurcation | Stronger or Weaker Effect as Move Away from Bifurcation, to Lowest Order. Unnormalized (Normalized by $FL^b$) |
|---|---|---|---|
| SNIPER | $\frac{1}{2\pi}\left[\frac{2\bar{I}c_{sn}}{\omega}\right]$ | $\sim \frac{1}{\omega}$ | Weaker (weaker) |
| Hopf | $\frac{1}{2\pi}\left[\frac{\bar{I}c_H}{\sqrt{|\omega-\omega_H|}}\right]$ | $\sim \frac{1}{\sqrt{|\omega-\omega_H|}}$ | Weaker (weaker) |
| Bautin | $\frac{1}{2\pi}\left[\frac{\bar{I}|c_B|}{|\omega-\omega_{SN}|}\right]$ | $\sim \frac{1}{|\omega-\omega_{SN}|}$ | Weaker (weaker) |
| Homoclinic | $\frac{1}{2\pi}\bar{I}c_{hc}\,\omega\exp\left(\frac{2\pi\lambda_u}{\omega}\right)$ | $\sim \omega\exp(k/\omega)$ | Weaker (weaker) |
| IF | $\bar{I}$ | const. | Constant (weaker) |
| LIF | $\frac{1}{2\pi}\frac{\bar{I}\omega}{g_L}\left(e^{2\pi g_L/\omega}-1\right)$ | $\sim \omega\exp(k/\omega)$ | Weaker (weaker) |

Note: The positive constant $k$ differs from case to case.

Table 4: Scaling of Deviations in Firing Rate During Stimulus $FL^d_{\min} - FL^b$ for the Different Neuron Models.

| Bifurcation | $FL^d_{\min} - FL^b$ | Lowest Order Scaling Near Bifurcation | Stronger or Weaker Effect as Move Away from Bifurcation, to Lowest Order. Unnormalized (Normalized by $FL^b$) |
|---|---|---|---|
| SNIPER | $0$ | Constant | Constant (constant) |
| Hopf | $-\frac{1}{2\pi}\left[\frac{\bar{I}c_H}{\sqrt{|\omega-\omega_H|}}\right]$ | $\sim -\frac{1}{\sqrt{|\omega-\omega_H|}}$ | Weaker (weaker) |
| Bautin | $-\frac{1}{2\pi}\left[\frac{\bar{I}|c_B|}{|\omega-\omega_{SN}|}\right]$ | $\sim -\frac{1}{|\omega-\omega_{SN}|}$ | Weaker (weaker) |
| Homoclinic | $\frac{1}{2\pi}\bar{I}c_{hc}\,\omega$ | $\sim \omega$ | Stronger (constant) |
| IF | $\bar{I}$ | Constant | Constant (weaker) |
| LIF | $\frac{1}{2\pi}\frac{\bar{I}\omega}{g_L}\left(1 - e^{-2\pi g_L/\omega}\right)$ | $\sim \omega$ | Stronger (constant) |

Table 5: Scaling of Deviations in Firing Rate After Stimulus, $FL^a_{\max} - FL^b$, for the Different Neuron Models.

| Bifurcation | $FL^a_{\max} - FL^b$ | Lowest Order Scaling Near Bifurcation | Stronger or Weaker Effect as Move Away from Bifurcation, to Lowest Order. Unnormalized (Normalized by $FL^b$) |
|---|---|---|---|
| SNIPER | $\frac{1}{2\pi}\left[\frac{2\bar{I}c_{sn}}{\omega}\right]$ | $\sim \frac{1}{\omega}$ | Weaker (weaker) |
| Hopf | $\frac{1}{2\pi}\left[\frac{2\bar{I}c_H\omega}{\omega\sqrt{|\omega-\omega_H|}-\bar{I}c_H}\right]$ | $\sim \frac{1}{\sqrt{|\omega-\omega_H|}}$ | Weaker (weaker) |
| Bautin | $\frac{1}{2\pi}\left[\frac{2\bar{I}|c_B|\omega}{\omega|\omega-\omega_{SN}|-\bar{I}|c_B|}\right]$ | $\sim \frac{1}{|\omega-\omega_{SN}|}$ | Weaker (weaker) |
| Homoclinic | $\frac{1}{2\pi}\frac{\bar{I}c_{hc}\omega}{1+\bar{I}c_{hc}}(\exp(2\pi\lambda_u/\omega)-1)$ | $\sim \omega\exp(k/\omega)$ | Weaker (weaker) |
| IF | $0$ | Constant | Constant (constant) |
| LIF | $\frac{\omega}{2\pi}\frac{\bar{I}(1-e^{-2\pi g_L/\omega})(e^{2\pi g_L/\omega}-1)}{g_L+\bar{I}(1-e^{-2\pi g_L/\omega})}$ | $\sim \omega\exp(k/\omega)$ | Weaker (weaker) |

Note: The positive constant $k$ differs from case to case.

Table 6: Scaling of Deviations in Firing Rate After Stimulus $FL_{\min}^a - FL^b$ for the Different Neuron Models.

| Bifurcation | $FL_{\min}^a - FL^b$ | Lowest Order Scaling Near Bifurcation | Stronger or Weaker Effect as Move Away from Bifurcation, to Lowest Order. Unnormalized (Normalized by $FL^b$) |
|---|---|---|---|
| SNIPER | $-\dfrac{1}{2\pi}\left[\dfrac{2\bar{I}c_{SN}}{\omega+2c_{sn}\bar{I}/\omega}\right]$ | $\sim -\omega$ | Stronger (constant) |
| Hopf | $-\dfrac{1}{2\pi}\left[\dfrac{2\bar{I}c_H\omega}{\omega\sqrt{|\omega-\omega_H|}+\bar{I}c_H}\right]$ | $\sim -\dfrac{1}{\sqrt{|\omega-\omega_H|}}$ | Weaker (weaker) |
| Bautin | $-\dfrac{1}{2\pi}\left[\dfrac{2\bar{I}|c_B|\omega}{\omega|\omega-\omega_{SN}|+\bar{I}|c_B|}\right]$ | $\sim -\dfrac{1}{|\omega-\omega_{SN}|}$ | Weaker (weaker) |
| Homoclinic | $\dfrac{\bar{I}c_{hc}\omega}{2\pi}\dfrac{\exp(-\frac{2\pi\lambda_u}{\omega})-1}{\exp(\frac{-2\pi\lambda_u}{\omega})+\bar{I}c_{hc}}$ | $\sim -\omega$ | Stronger (constant) |
| IF | $0$ | Constant | Constant (constant) |
| LIF | $\dfrac{\omega}{2\pi}\dfrac{\bar{I}(e^{2\pi g_L/\omega}-1)(e^{-2\pi g_L/\omega}-1)}{g_L+\bar{I}(e^{2\pi g_L/\omega}-1)}$ | $\sim -\omega$ | Stronger (constant) |

## 5 Gain of Oscillator Populations

In attempts to understand neural information processing, it is useful to understand how input signals are modified by transmission through various populations of spiking cells in different brain organs. The general way to treat this problem is by transfer functions (Servan-Schreiber, Printz, & Cohen, 1990; Gerstner & Kistler, 2002). Here we interpret the results of the previous section in terms of the amplification, or attenuation, of step function input stimuli by the neural population. We consider both extremal and average values of the firing rate $FL(t)$ during stepped stimuli of varying strengths and illustrate for neurons near a SNIPER bifurcation. We will use the word gain to describe the sensitivity of the resulting input-output relationship: systems with higher gain have a greater output range for a specific set of input strengths. The average firing rate during stimulus is

$$\langle FL^d \rangle \equiv \frac{1}{P}, \tag{5.1}$$

where $P$ is the period of an individual oscillator during the stimulus (see equation 4.9), and $\langle \cdot \rangle$ is the average over one such period. For the special

case of a population near a SNIPER bifurcation, $P_{SN} = \frac{2\pi}{\sqrt{\omega^2 + 2c_{sn}I}}$, so that

$$\langle FL_{SN}^d \rangle = \frac{\sqrt{\omega^2 + 2c_{sn}I}}{2\pi}. \tag{5.2}$$

These expressions describe the standard $f - I$ curve typically studied for single neurons (Rinzel & Ermentrout, 1998).

The instantaneous responses of neurons are in some cases of greater interest than averages such as equations 5.1 and 5.2. To derive the extremal (i.e., maximally above or below baseline) firing rates, we appeal to expressions 4.11 and 4.12, which are valid for both positive and negative values of $\bar{I}$ as long as $v(\theta, t)$ remains nonnegative. (However, the subsequent formulas of section 4.2 require modification: max and min must be appropriately interchanged when dealing with negative $\bar{I}$.) Thus, the extremal value of $FL^d(t)$ is (cf. equation 4.13)

$$FL^{d,ext} = \frac{1}{2\pi}[\omega + \bar{I}z_{\max}], \tag{5.3}$$

in general, and in particular for the SNIPER bifurcation:

$$FL_{SN}^{d,ext} = \frac{1}{2\pi}\left[\omega + \frac{2c_{sn}\bar{I}}{\omega}\right]. \tag{5.4}$$

In Figure 8, we plot $FL_{SN}^{ext}$ as a function of both baseline firing rate and stimulus strength $\bar{I}$, where the latter takes both positive and negative values. For (here, negative) stimulus values, and frequencies, sufficient to cause the minimum of $v(\theta)$ to dip below zero, fixed points appear in the phase model, giving firing rates $FL^d(t) = \langle FL_{SN}^d \rangle = FL_{SN}^{d,ext} = 0$. Notice the increased sensitivity of extremal firing rates to changes in stimulus strength at low baseline frequencies. This "increased gain" is also shown in Figure 9a, which plots slices through Figure 8 for two different baseline frequencies. However, there is no analogous effect for the average firing rates of equation 5.2, which follow the standard frequency-current relationships for individual neurons (see Figure 9b).

Note that there is always a crossing point between firing rate curves for near-SNIPER populations with high and low baseline frequencies (see Figure 9a). Above this crossing point, stimuli are more greatly amplified by the low-frequency population; below the crossing point, they are more greatly amplified by the high-frequency population. This is analogous to increasing the slope (= gain) of a sigmoidal response function as in Servan-Schreiber et al. (1990), gain increase in Figure 1 of that article being analogous to decrease of $\omega$. Thus, if signal discrimination depends on extremal firing rates, the effects of gain modulation on signal and noise discrimination of Servan-Schreiber et al. (1990) could be produced by changes in baseline rate.
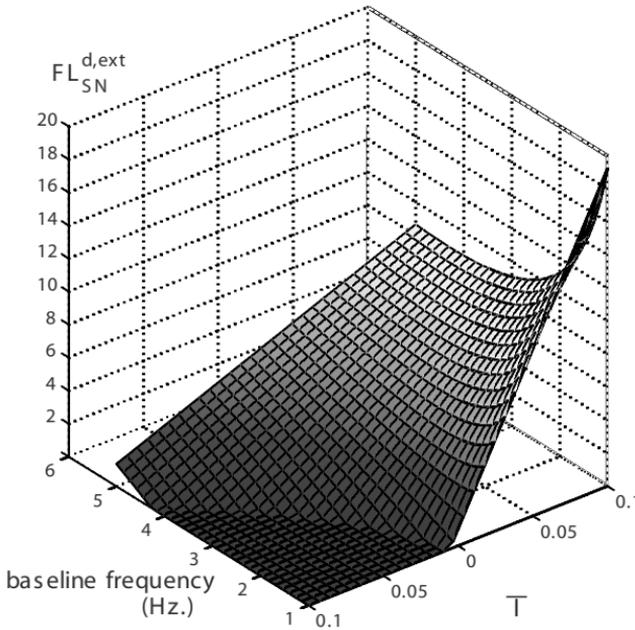
Figure 8: Maximum and minimum firing rate $FL_{SN}^{d,ext}$ of a population of stimulated HR neurons in Hz, as a function of baseline frequency (Hz) and applied current strength $\bar{I}$ ($\mu$A/cm$^2$).

## 6 Discussion

We now provide further comments on how the mechanisms studied in this article could be applied and tested. As discussed in section 5 and with regard to the locus coeruleus (LC) in section 1, baseline frequency-dependent variations in the sensitivity of neural populations to external stimuli could be used to adjust gain in information processing. The effect could be to engage the processing units relevant to specific tasks, and as in Servan-Schreiber et al. (1990) and Usher et al. (1999), to additionally sensitize these units to salient stimuli. See Brown et al. (2003b) for details of the LC application.

We recall that section 4.2 described the different types of poststimulus ringing of firing rates $FL(t)$ that occur for the various neuron models. This phase-resetting effect has long been studied in theoretical and experimental neuroscience (e.g. Winfree, 2001; Tass, 1999; Makeig et al., 2002). As we show here (see equation 4.19 and Figure 7), for neuron models having a phase response curve $z(\theta)$ that takes negative values, the greatest deviations from baseline firing rates can occur significantly *after* stimulus end. Subpopulations of such neurons could be used in detecting termination of sensory stimuli. Elevated firing rates $FL(t)$ that remain (or are enhanced)
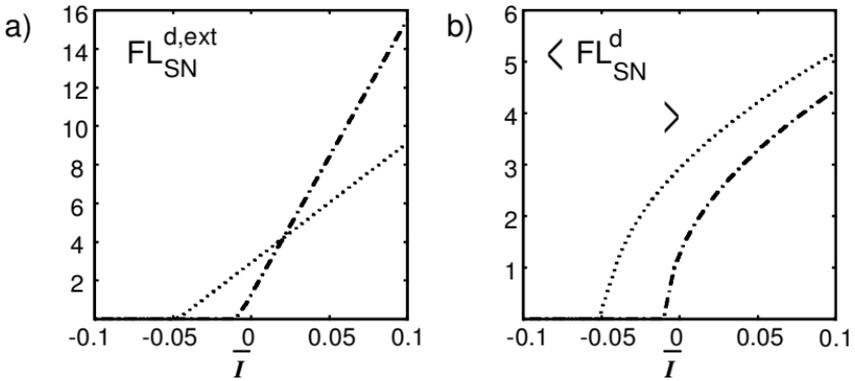
Figure 9: Maximum and minimum firing rate of a population of stimulated HR neurons (a) and average firing rate (b) in Hz, as a function of applied current strength for two different baseline frequencies: 1.3 Hz (dot-dashed line) and the higher-frequency 2.9 Hz (dotted line). The increased gain effect at lower baseline frequencies discussed is evident for maximum and minimum, but not average, firing rates (see the text).

after the stimulus ends are an example of persistent neural activity, a general phenomenon implicated in short-term memory, interval timing, and other functions. However, physiological evidence suggests that some of the persistent activity observed *in vivo* results from desynchronized, not phase-clustered, neural groups.

Finally, stimulus-induced ringing of population firing rates (which occurs at the natural baseline frequency of the neuron population; see equation 4.6) could play a role in generating alpha-wave patterns ("alpha-ringing"); the possible relevance of this effect is well known and is a topic of current debate in the EEG community (Makeig et al., 2002; Bogacz, Yeung, & Holroyd, 2002).

The results presented here are experimentally testable. As noted in section 1, the predictions for average firing rate $FL(t)$ are equally valid for multi-channel recordings from a (weakly coupled) population and for sequences of single-unit recordings from members of such a population. Thus, the $FL(t)$ predictions of this article can be compared with PSTHs formed from both types of data. The scaling of response magnitudes predicted in section 4.3 could be tested in any experiment in which baseline neural firing rates are modulated pharmacologically while stereotyped stimuli are presented. This is essentially what is done in many experiments on the effects of different neuromodulators, neurotransmitters, and other agents. For example, direct application of the neuropeptide corticotropin releasing factor (CRF) has been found to increase LC baseline activity and simultaneously decrease responses to sensory stimuli (Moore & Bloom, 1979) in some, but

not all, protocols. Many other examples of such modulatory effects of neu-
rotransmitters or exogenous inputs exist for neurons in other brain areas
(Aston-Jones et al., 2001). However, a general difficulty is that these sub-
stances may change many parameters in neurons besides the bifurcation
parameter $I_b$ that is the focus of this article, making it difficult to determine
what mechanism leads to changes in averaged response. Furthermore, the
presence of noise tends to diminish the scaling results reported here (cf.
Herrmann & Gerstner, 2001; Brown et al., 2003b), and while it seems that
coupling can in some circumstances amplify the scaling (Brown et al., 2003b),
we are still working to clarify this effect.

We close by mentioning another experimental test of the predictions pre-
sented here, suggested by John Rinzel. First, one could determine what
pharmacological manipulations would cause a given *in vitro* neuron to tran-
sition from periodic firing near a SNIPER bifurcation to periodic firing near
a Bautin bifurcation. Then one could measure how trial-averaged responses
to stereotyped stimuli vary as this manipulation is performed. In particu-
lar, this article predicts that maximal responses should occur during the
stimulus in SNIPER firing, but after the stimulus switches off following a
manipulation to Bautin firing.

## Appendix A: The Adjoint Method

Consider an infinitesimal perturbation $\Delta \mathbf{x}$ to the trajectory $\mathbf{x}^\gamma(t) \in \gamma$ at time
$t = 0$. Let $\mathbf{x}(\mathbf{t})$ be the trajectory evolving from this perturbed initial condition.
Defining $\Delta \mathbf{x}(\mathbf{t})$ via $\mathbf{x}(\mathbf{t}) = \mathbf{x}^\gamma(\mathbf{t}) + \Delta \mathbf{x}(\mathbf{t})$,

$$\frac{d\Delta \mathbf{x}(t)}{dt} = DF(\mathbf{x}^\gamma(\mathbf{t}))\Delta \mathbf{x}(\mathbf{t}) + \mathcal{O}(\|\Delta \mathbf{x}\|^2), \qquad \Delta \mathbf{x}(0) = \Delta \mathbf{x}. \tag{A.1}$$

For the phase shift defined as $\Delta\theta = \theta(\mathbf{x}(\mathbf{t})) - \theta(\mathbf{x}^\gamma(\mathbf{t}))$, we have

$$\Delta\theta = \langle \nabla_{\mathbf{x}^\gamma(t)}\theta, \Delta \mathbf{x}(t) \rangle + \mathcal{O}(\|\Delta \mathbf{x}\|^2), \tag{A.2}$$

where $\langle \cdot, \cdot \rangle$ defines the standard inner product (written as a dot product in
the main text), and $\nabla_{\mathbf{x}^\gamma(t)}\theta$ is the gradient of $\theta$ evaluated at $\mathbf{x}^\gamma(t)$. We recall
from above that $\Delta\theta$ is independent of time (after the perturbation at $t = 0$)
so that taking the time derivative of equation A.2 yields, to lowest order in
$\|\Delta \mathbf{x}\|$,

$$\left\langle \frac{d\nabla_{\mathbf{x}^\gamma(t)}\theta}{dt}, \Delta \mathbf{x}(t) \right\rangle = -\left\langle \nabla_{\mathbf{x}^\gamma(t)}\theta, \frac{d\Delta \mathbf{x}(t)}{dt} \right\rangle$$

$$= -\langle \nabla_{\mathbf{x}^\gamma(t)}\theta, DF(\mathbf{x}^\gamma(\mathbf{t}))\,\Delta \mathbf{x}(\mathbf{t}) \rangle$$

$$= -\langle DF^T(\mathbf{x}^\gamma(\mathbf{t}))\,\nabla_{\mathbf{x}^\gamma(\mathbf{t})}\theta, \Delta \mathbf{x}(\mathbf{t}) \rangle. \tag{A.3}$$

Here the matrix $DF^T(\mathbf{x}^\gamma(\mathbf{t}))$ is the transpose (i.e., adjoint) of the (real) matrix $DF(\mathbf{x}^\gamma(\mathbf{t}))$. Since the above equalities hold for arbitrary perturbations $\Delta\mathbf{x}(t)$, we have

$$\frac{d\nabla_{\mathbf{x}^\gamma(t)}\theta}{dt} = -DF^T(\mathbf{x}^\gamma(t))\,\nabla_{\mathbf{x}^\gamma(t)}\theta. \tag{A.4}$$

Finally, recall that from equation 2.4 that

$$\frac{d\theta}{dt} = \nabla_{\mathbf{x}}\theta \cdot \frac{d\mathbf{x}}{dt} = \nabla_{\mathbf{x}}\theta \cdot F(\mathbf{x}) = \omega, \tag{A.5}$$

which in particular must hold at $t = 0$. Thus, as in Hoppensteadt and Izhikevich (1997), Ermentrout (2002), and Ermentrout and Kopell (1991), we must solve equation A.4 subject to the condition

$$\nabla_{\mathbf{x}^\gamma(0)}\theta \cdot F(\mathbf{x}^\gamma(0)) = \omega. \tag{A.6}$$

Since $\nabla_{\mathbf{x}^\gamma(t)}\theta$ evolves in $\mathbb{R}^N$, equation A.6 supplies only one of $N$ required initial conditions; the rest arise from requiring that the solution $\nabla_{\mathbf{x}^\gamma(t)}\theta$ to equation A.4 be $T$-periodic (Hoppensteadt & Izhikevich, 1997; Ermentrout, 2002; Ermentrout & Kopell, 1991).

Note that equations A.4 and A.6 correspond to equations 9.16 and 9.17 of Hoppensteadt and Izhikevich (1997), with the identification of $\nabla_{\mathbf{x}}\theta \to Q$ and a slightly different parameterization. Indeed, this is the adjoint problem that XPP solves to numerically find the PRC $Q_{\mathrm{XPP}}$. The relationship is

$$\nabla_{\mathbf{x}}\theta = \omega Q_{\mathrm{XPP}}. \tag{A.7}$$

## Appendix B: The Strong Attraction Method

The "strong attraction limit" of a coordinate change to the phase variable $\theta_2$ discussed in Ermentrout and Kopell (1990) and Hoppensteadt and Izhikevich (1997) effectively sets

$$\frac{\partial\theta_2}{\partial\mathbf{x}}(\mathbf{x}) = \frac{F(\mathbf{x})}{\|F(\mathbf{x})\|^2}\omega, \tag{B.1}$$

which clearly satisfies equation 2.4 but implicitly imposes $N-1$ additional constraints. In particular, level sets of $\theta_2$ are always orthogonal to $\gamma$, which is not generally the case for isochrons. Furthermore, equation B.1 requires that $\frac{F(\mathbf{x})}{\|F(\mathbf{x})\|^2}\omega$ is the gradient of the scalar function $\theta_2$, which is possible only if it is curl free in a neighborhood of $\gamma$. Since it is proportional to the unit-normalized vector field, which exhibits the attracting limit cycle, $\frac{F(\mathbf{x})}{\|F(\mathbf{x})\|^2}\omega$ will never meet this requirement, so the phase variable $\theta_2$ cannot be extended

to a neighborhood of $\gamma$. More practically, $\frac{\partial\theta}{\partial\mathbf{x}}(\mathbf{x}^\gamma)$ and $\frac{\partial\theta_2}{\partial\mathbf{x}}(\mathbf{x}^\gamma)$ can also give qualitatively different phase dynamics, with $\theta$ dynamics representing more accurately the original full equations. See Brown et al. (2003a) for an example involving the stability of phase-locked states in coupled Hodgkin-Huxley systems.

**Appendix C: Equations for the Neural Models** ───────────

**Rose-Hindmarsh Equations**

$$\dot{V} = [I^b - g_{Na}m_\infty(V)^3(-3(q - Bb_\infty(V)) + 0.85)(V - V_{Na})$$
$$-g_K q(V - V_K) - g_L(V - V_L)]/C$$
$$\dot{q} = (q_\infty(V) - q)/\tau_q(V)$$
$$q_\infty(V) = n_\infty(V)^4 + Bb_\infty(V), \quad b_\infty(V) = (1/(1 + \exp(\gamma_b(V + 53.3))))^4,$$
$$m_\infty(V) = \alpha_m(V)/(\alpha_m(V) + \beta_m(V)),$$
$$n_\infty(V) = \alpha_n(V)/(\alpha_n(V) + \beta_n(V)),$$
$$\tau_q(V) = (\tau_b(V) + \tau_n(V))/2, \quad \tau_n(V) = T_n/(\alpha_n(V) + \beta_n(V)),$$
$$\tau_b(V) = T_b(1.24 + 2.678/(1 + \exp((V + 50)/16.027))),$$
$$\alpha_n(V) = 0.01(V + 45.7)/(1 - \exp(-(V + 45.7)/10)),$$
$$\alpha_m(V) = 0.1(V + 29.7)/(1 - \exp(-(V + 29.7)/10)),$$
$$\beta_n(V) = 0.125\exp(-(V + 55.7)/80),$$
$$\beta_m(V) = 4\exp(-(V + 54.7)/18).$$

Parameters:

$$V_{Na} = 55 \text{ mV}, \ V_K = -72 \text{ mV}, \ V_L = -17 \text{ mV}, \ g_{Na} = 120 \text{ mS/cm}^2,$$
$$g_K = 20 \text{ mS/cm}^2, \ g_L = 0.3 \text{ mS/cm}^2, \ g_A = 47.7 \text{ mS/cm}^2,$$
$$C = 1 \ \mu\text{F/cm}^2, \ I_i^b = 5 \ \mu\text{A/cm}^2, \ \gamma_b = 0.069 \text{ mV}^{-1},$$
$$T_b = 1 \text{ msec}, \ T_n = 0.52 \text{ msec}, \ B = 0.21 \, g_A/g_K.$$

**Fitzhugh-Nagumo Equations**

$$\dot{V} = [-w - V(V - 1)(V - a) + I^b]/C$$
$$\dot{w} = \epsilon(V - g_a w)$$

Parameters:

$$g_a = 1, \ \epsilon = 0.05, \ a = 0.1 \text{ mV}, \ C = 1 \ \mu\text{F/cm}^2.$$

## Hodgkin-Huxley Equations

$$dV/dt = 1/C(I - g_{Na}h(V - V_{Na})m^3 - g_K(V - V_K)n^4 - g_L(V - V_L))$$
$$dm/dt = a_m(V)(1 - m) - b_m(V)m$$
$$dh/dt = a_h(V)(1 - h) - b_h(V)h$$
$$dn/dt = a_n(V)(1 - n) - b_n(V)n$$
$$a_m(V) = 0.1(V + 40)/(1 - \exp(-(V + 40)/10))$$
$$b_m(V) = 4\exp(-(V + 65)/18)$$
$$a_h(V) = 0.07\exp(-(V + 65)/20)$$
$$b_h(V) = 1/(1 + \exp(-(V + 35)/10))$$
$$a_n(V) = 0.01(V + 55)/(1 - \exp(-(V + 55)/10))$$
$$b_n(V) = 0.125\exp(-(V + 65)/80)$$

Parameters:

$$V_{Na} = 50 \text{ mV}, \; Vk = -77 \text{ mV}, \; V_L = -54.4 \text{ mV},$$
$$g_{Na} = 120 \text{ mS/cm}^2$$
$$g_K = 36 \text{ mS/cm}^2, \; g_L = .3 \text{ mS/cm}^2, \; C = 1 \; \mu\text{F/cm}^2.$$

## Morris-Lecar Equations

$$\dot{V} = [g_{Ca}m_\infty(V)(V_{Ca} - V) + g_K w(V_K - V) + g_L(V_L - V) + I^b]/C$$
$$\dot{w} = \phi(w_\infty(V) - w)/\tau_w(V)$$
$$m_\infty(V) = 0.5(1 + \tanh((V - V_1)/V_2))$$
$$w_\infty(V) = 0.5(1 + \tanh((V - V_3)/V_4))$$
$$\tau_w(V) = 1/\cosh((V - V_3)/(2V_4))$$

Parameters:

$$\phi = 0.23, \; g_L = 2 \text{ mS/cm}^2, \; g_{Ca} = 4 \text{ mS/cm}^2, \; g_K = 8 \text{ mS/cm}^2,$$
$$C = 20 \; \mu\text{F/cm}^2$$
$$V_K = -84 \text{ mV}, \; V_L = -60 \text{ mV}, \; V_{Ca} = 120 \text{ mV}$$
$$V_1 = -1.2 \text{ mV}, \; V_2 = 18 \text{ mV}, \; V_3 = 12 \text{ mV}, \; V_4 = 17.4 \text{ mV}$$

## Acknowledgments

**References**

Aston-Jones, G., Chen, S., Zhu, Y., & Oshinsky, M. (2001). A neural circuit for circadian regulation of arousal. *Nature Neurosci., 4*, 732–738.

Aston-Jones, G., Rajkowski, J., & Cohen, J. (2000). Locus coeruleus and regulation of behavioral flexibility and attention. *Prog. Brain Res., 126*, 165–182.

Aston-Jones, G., Rajkowski, J., Kubiak, P., & Alexinsky, T. (1994). Locus coeruleus neurons in the monkey are selectively activated by attended stimuli in a vigilance task. *J. Neurosci., 14*, 4467–4480.

Bogacz, R., Yeung, N., & Holroyd, C. (2002). *Detection of phase resetting in the electroencephalogram: An evaluation of methods.* Abstract, Society for Neuroscience, Washington DC.

Bressloff, P., & Coombes, S. (2000). Dynamics of strongly coupled spiking neurons. *Neural Comp., 12*, 91–129.

Brown, E., Holmes, P., & Moehlis, J. (2003a). Globally coupled oscillator networks. In E. Kaplan, J. Marsden, & K. Sreenivasan (Eds.), *Problems and perspectives in nonlinear science, A celebratory volume in honor of Lawrence Sirovich* (pp. 183–215). New York: Springer-Verlag.

Brown, E., Moehlis, J., Holmes, P., Clayton, E., Rajkowski, J., & Aston-Jones, G. (2003b). *The influence of spike rate and stimulus duration on noradrenergic neurons.* Unpublished manuscript, Program in Applied and Computational Mathematics, Princeton University.

Brunel, N., Chance, F., Fourcaud, N., & Abbott, L. (2001). Effects of synaptic noise and filtering on the frequency response of spiking neurons. *Phys. Rev. Lett., 86*, 2186–2189.

Casti, A., Omurtag, A., A., S., Kaplan, E., Knight, B., Sirovich, L., & Victor, J. (2001). A population study of integrate-and-fire-or-burst neurons. *Neural Comp., 14*, 957–986.

Coddington, E., & Levinson, N. (1955). *Theory of ordinary differential equations.* New York: McGraw-Hill.

Eckhorn, R. (1999). Neural mechanisms of scene segmentation: Recordings from the visual cortex suggest basic circuits for linking field models. *IEEE Trans. Neural Networks, 10*, 464–479.

Ermentrout, G. (1981). $n : m$ phase locking of weakly coupled oscillators. *J. Math. Biol., 12*, 327–342.

Ermentrout, G. (1996). Type I membranes, phase resetting curves, and synchrony. *Neural Comp., 8*, 979–1001.

Ermentrout, G. (2002). *Simulating, analyzing, and animating dynamical systems: A guide to XPPAUT for researchers and students.* Philadelphia: SIAM.

Ermentrout, G., & Kopell, N. (1984). Frequency plateaus in a chain of weakly coupled oscillators, I. *SIAM J. Math. Anal., 15*, 215–237.

Ermentrout, G., & Kopell, N. (1990). Oscillator death in systems of coupled neural oscillators. *SIAM J. Appl. Math., 50*, 125–146.

Ermentrout, G., & Kopell, N. (1991). Multiple pulse interactions and averaging in coupled neural oscillators. *J. Math. Biol., 29*, 195–217.

Evans, L. (1998). *Partial differential equations.* Providence, RI: American Mathematical Society.

Fenichel, N. (1971). Persistence and smoothness of invariant manifolds for flows. *Ind. Univ. Math. J., 21*, 193–225.

Fetz, E., & Gustaffson, B. (1983). Relation between shapes of post-synaptic potentials and changes in firing probability of cat motoneurones. *J. Physiol., 341*, 387–410.

Fourcaud, N., & Brunel, N. (2002). Dynamics of the firing probability of noisy integrate-and-fire neurons. *Neural Comp., 14*, 2057–2110.

Gerstner, W. (2000). Population dynamics of spiking neurons: Fast transients, synchronous states, and locking. *Neural Comp., 12*, 43–89.

Gerstner, W., & Kistler, W. (2002). *Spiking neuron models*. Cambridge: Cambridge University Press.

Gerstner, W., van Hemmen, L., & Cowan, J. (1996). What matters in neuronal locking? *Neural Comp., 8*, 1653–1676.

Glass, L., & Mackey, M. (1988). *From Clocks to chaos*. Princeton, NJ: Princeton Paperbacks.

Gray, C. (2000). The temporal correlation hypothesis of visual feature integration: Still alive and well. *Neuron, 24*, 31–47.

Guckenheimer, J. (1975). Isochrons and phaseless sets. *J. Math. Biol., 1*, 259–273.

Guckenheimer, J., & Holmes, P. (1983). *Nonlinear oscillations, dynamical systems and bifurcations of vector fields*. New York: Springer-Verlag.

Hansel, D., Mato, G., & Meunier, C. (1993). Phase dynamics for weakly coupled Hodgkin-Huxley neurons. *Europhys. Lett., 25*(5), 367–372.

Hansel, D., Mato, G., & Meunier, C. (1995). Synchrony in excitatory neural networks. *Neural Comp., 7*, 307–337.

Herrmann, A., & Gerstner, W. (2001). Noise and the PSTH response to current transients: I. General theory and application to the integrate-and-fire neuron. *J. Comp. Neurosci., 11*, 135–151.

Hirsch, M., Pugh, C., & Shub, M. (1977). *Invariant manifolds*. New York: Springer-Verlag.

Hodgkin, A., & Huxley, A. (1952). A quantitative description of membrane current and its application to conduction and excitation in nerve. *J. Physiol., 117*, 500–544.

Hoppensteadt, F., & Izhikevich, E. (1997). *Weakly connected neural networks*. New York: Springer-Verlag.

Izhikevich, E. (2000a). Neural excitability, spiking and bursting. *Int. J. Bif. Chaos, 10*, 1171–1266.

Izhikevich, E. (2000b). Phase equations for relaxation oscillators. *SIAM J. Appl. Math., 60*, 1789–1804.

Keener, J., & Sneyd, J. (1998). *Mathematical physiology*. New York: Springer-Verlag.

Kim, S., & Lee, S. (2000). Phase dynamics in the biological neural networks. *Physica D, 288*, 380–396.

Kuramoto, Y. (1984). *Chemical oscillations, waves, and turbulence*. Berlin: Springer-Verlag.

Kuramoto, Y. (1997). Phase- and center-manifold reductions for large populations of coupled oscillators with application to non-locally coupled systems. *Int. J. Bif. Chaos, 7*, 789–805.

Kuznetsov, Y. (1998). *Elements of applied bifurcation theory* (2nd ed.). New York: Springer-Verlag.

Lewis, T., & Rinzel, J. (2003). Dynamics of spiking neurons connected by both inhibitory and electrical coupling. *J. Comp. Neurosci., 14*, 283–309.

Mainen, Z., & Sejnowski, T. (1995). Reliability of spike timing in neocortical neurons. *Science, 268*, 1503–1506.

Makeig, S., Westerfield, M., Jung, T.-P., Enghoff, S., Townsend, J., Courchesne, E., & Sejnowski, T. (2002). Dynamic brain sources of visual evoked responses. *Science, 295*, 690–694.

Malkin, I. (1949). *Methods of Poincaré and Liapunov in the theory of nonlinear oscillations.* Moscow: Gostexizdat.

Matell, M., & Meck, W. (2000). Neurophysiological mechanisms of interval timing behavior. *BioEssays, 22*, 94–103.

Moore, R., & Bloom, F. (1979). Central catecholamine neuron systems: Anatomy and physiology of the norepinephrine and epinephrine systems. *Ann. Rev. Neurosci., 2*, 113–168.

Murray, J. (2002). *Mathematical biology I: An introduction.* (3rd ed.). New York: Springer-Verlag.

Nykamp, D., & Tranchina, D. (2000). A population density approach that facilitates large-scale modeling of neural networks: Analysis and application to orientation tuning. *J. Comp. Neurosci., 8*, 19–50.

Omurtag, A., Knight, B., & Sirovich, L. (2000). On the simulation of large populations of neurons. *J. Comp. Neurosci., 8*, 51–63.

Rinzel, J., & Ermentrout, G. (1998). Analysis of neural excitability and oscillations. In C. Koch & I. Segev (Eds.), *Methods in neuronal modeling* (pp. 251–291). Cambridge, MA: MIT Press.

Rinzel, J., & Miller, R. (1980). Numerical calculations of stable and unstable periodic solutions to the Hodgkin-Huxley equations. *Math. Biosci., 49*, 27–59.

Ritt, J. (2003). *A probabilistic analysis of forced oscillators, with application to neuronal response reliability.* Unpublished doctoral dissertation, Boston University.

Rose, R., & Hindmarsh, J. (1989). The assembly of ionic currents in a thalamic neuron I. The three-dimensional model. *Proc. R. Soc. Lond. B, 237*, 267–288.

Servan-Schreiber, D., Printz, H., & Cohen, J. (1990). A network model of catecholamine effects: Gain, signal-to-noise ratio, and behavior. *Science, 249*, 892–895.

Stein, R. (1965). A theoretical analysis of neuronal variability. *Biophys. J., 5*, 173–194.

Strogatz, S. (2000). From Kuramoto to Crawford: Exploring the onset of synchronization in populations of coupled oscillators. *Physica D, 143*, 1–20.

Tass, P. (1999). *Phase resetting in medicine and biology.* New York: Springer-Verlag.

Usher, M., Cohen, J., Servan-Schreiber, D., Rajkowsky, J., & Aston-Jones, G. (1999). The role of locus coeruleus in the regulation of cognitive performance. *Science, 283*, 549–554.

van Vreeswijk, C., Abbot, L., & Ermentrout, G. (1994). When inhibition not excitation synchronizes neural firing. *J. Comp. Neurosci., 1*, 313–321.

Whitham, G. (1974). *Linear and nonlinear waves.* New York: Wiley.

Wilson, H., & Cowan, J. (1972). Excitatory and inhibitory interactions in localized populations of model neurons. *Biophys. J., 12*, 1–24.

Winfree, A. (1974). Patterns of phase compromise in biological cycles. *J. Math. Biol., 1*, 73–95.

Winfree, A. (2001). *The geometry of biological time.* Second Edition. New York: Springer-Verlag.